

· //

”



”

“

“

”

:

•

-

:

•

, 2024 .

I.

COVID-19 (-19) , SARS-CoV-2 ,
(WHO-World Health Organization) 2020 ., 774 , 7

SARS-CoV-2 , ACE2, Neuropili-1, L-SIGN, CD147

SARS-CoV-2 Spike (S) S ,

L-cathepsin. TMPRSS2

Nucleocapsid (N) (ERGIC).

SARS-CoV-2

(virus-like particles-VLPs),

SARS-CoV-2.

embrane (M)

N

pH,

pH

Nikon Eclipse Ti2-E
(SPARTACUSS),

“Andor Dragonfly

HeLa Kyoto,
CLASPIN, RIF1 PCNA,

EGFP-ORC1, MCM6,
mCherry PCNA.

Nikon Eclipse Ti-E

Andor Revolution
Nikon Perfect Focus System (PFS).

II.

1. SARS-CoV-2
2. SARS-CoV-2
- 1.1. SARS-CoV-2
- 1.2. 3D
- 1.3. pH SARS-CoV-2
- 1.4. SARS-CoV-2
- 1.5. pH, SARS-CoV-2
- 2.1. RIF1, PCNA ORC1, MCM6, CLASPIN,

III.

IV.

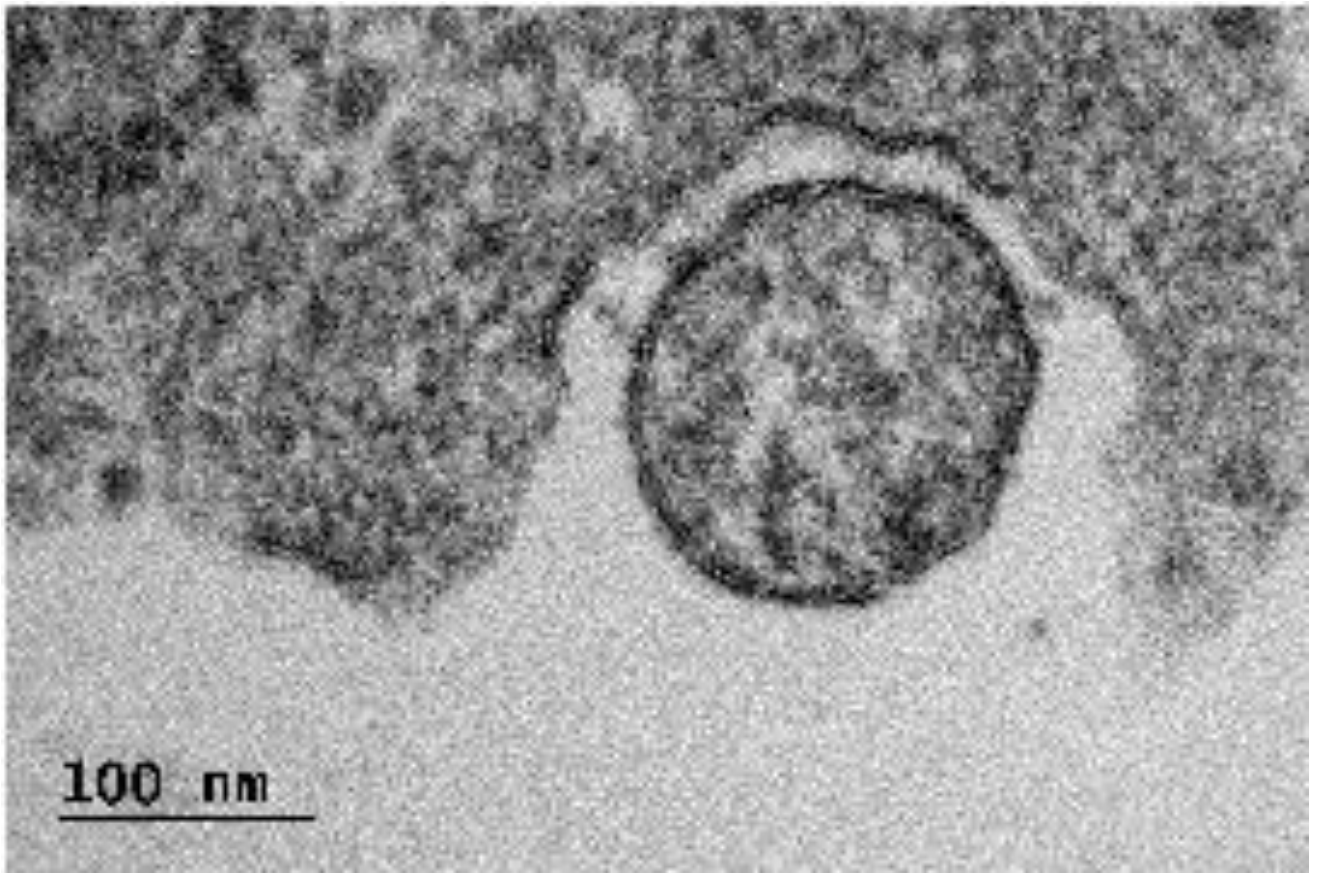
1.

1.1.

12.) , S (Wuhan) SARS-CoV-2 ,
SARS-CoV-2 HEK293 (,
SARS-CoV-2 13. ,
SARS-CoV-2 3,14. ,
S TEM (Transmission emission
microscopy) MLE-12 (. 1) ¹.

¹ *

TEM



100 nm

1.

SARS-CoV-2^{Wu}: (E,

S, M)
(MLE).

S

mCherry

4.

VLP^{Wu}:M^{Ch},

(VLP^{Wuhan}: (E, S, M&M-mCherry).

U2OS (),

ACE2,

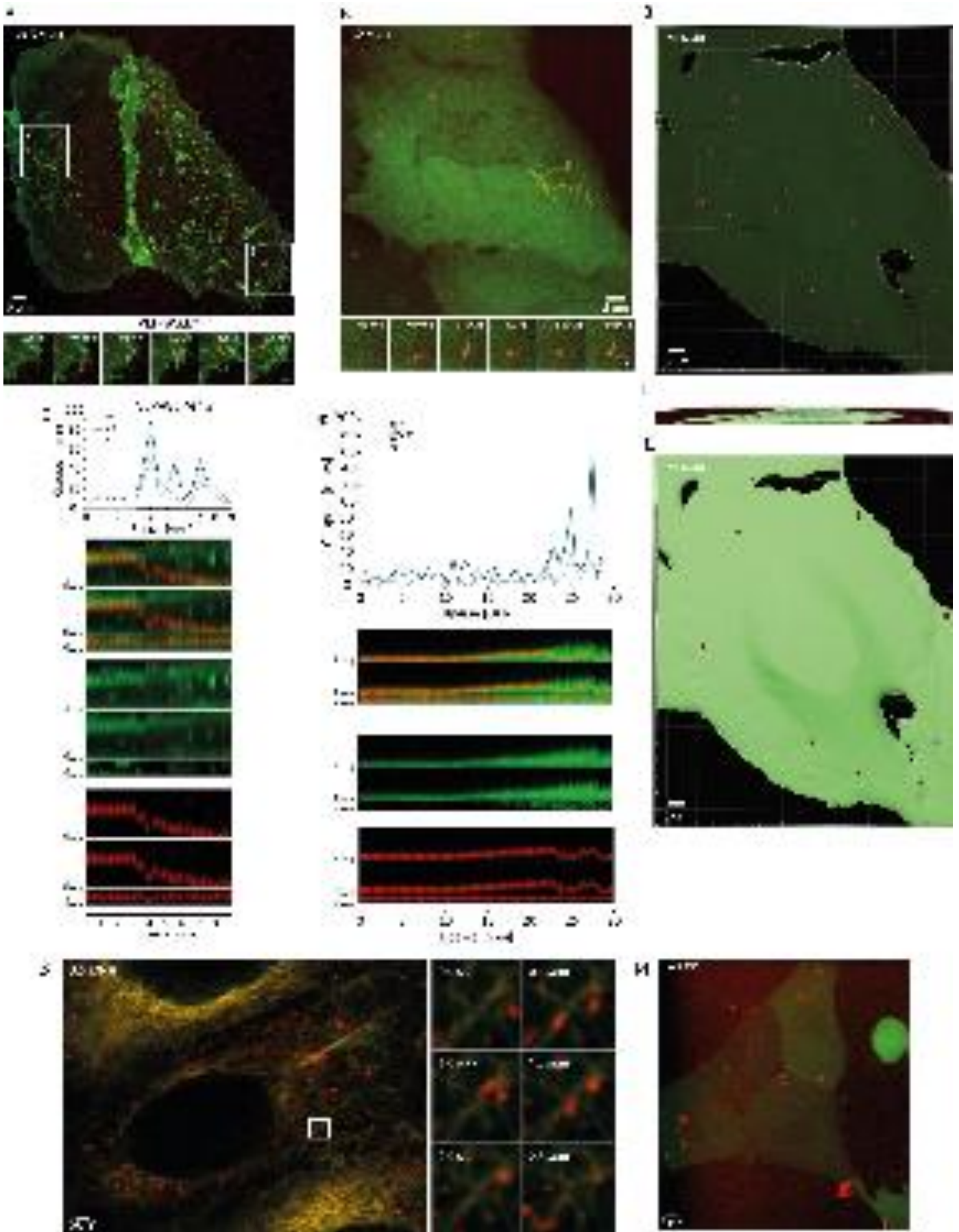
TMPRSS2,

NeonGreen ACE2

3D

30

(. 2)¹⁵.



2. CoV-2 - SARS-

SARS-CoV-2 VLP^{Wu}:M^{Ch} U2OS
 ACE2-NeonGreen TMPRSS2.
 , a

U2OS VLP^{Wu}:M^{Ch} mNeonGreen (),
 3D U2OS
 ()
 ()
 (), 3D VLP^{Wu}:M^{Ch}
 ()
 (2) ().

1D- (Z), 2D (XY) 3D (XYZ).
 (), ().
 Tubulin 610, (cabazitaxel),
 VLP^{Wu}:M^{Ch} (Wuhan)
 SARS-CoV-2.

(tracking),
 (.7).
 3D
 Python Fiji.

SPARTACUSS (Single PARTicle Tracking Analysis in Cells Using Software Solutions).

(,).
 SPARTACUSS,
 Gaussian blur, (.3). X Y
 Z .
 maximum intensity projection : maximum intensity x -
 z y; maximum intensity y -

z x; maximum intensity z -

x y.

() (.3 ,).
488 (), 591 ()
(.3).

SPARTACUSS

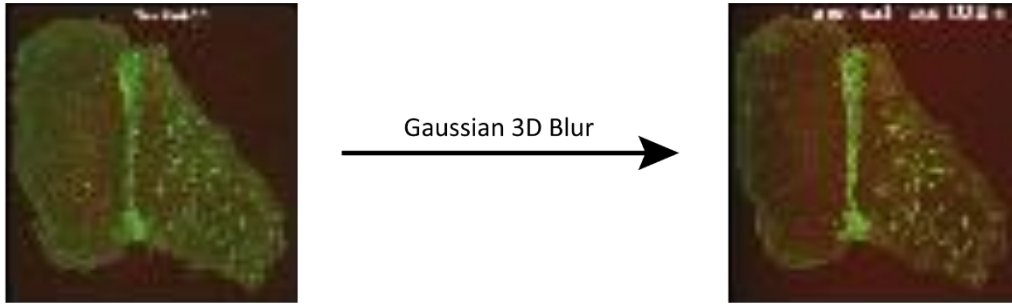
:

3D

(x,y,z)

() (.3).

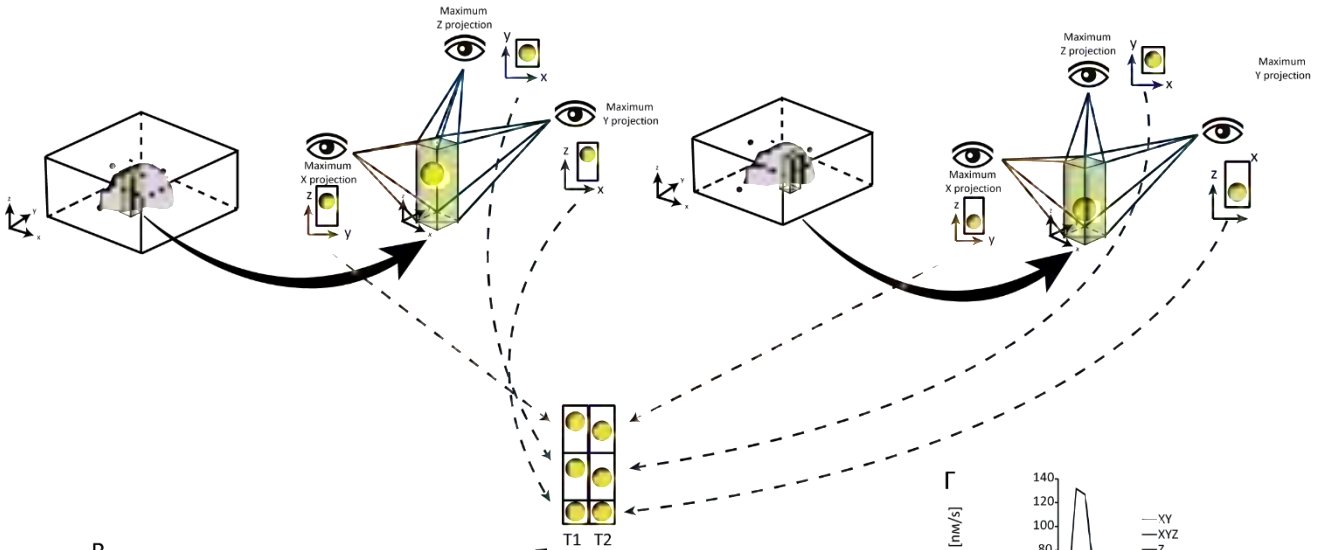
A



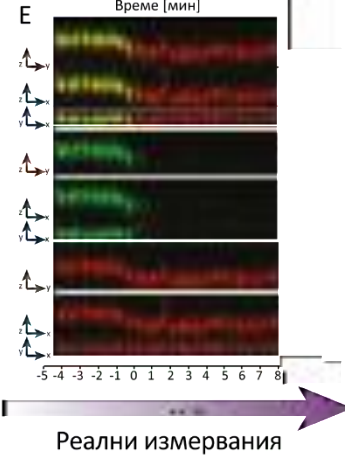
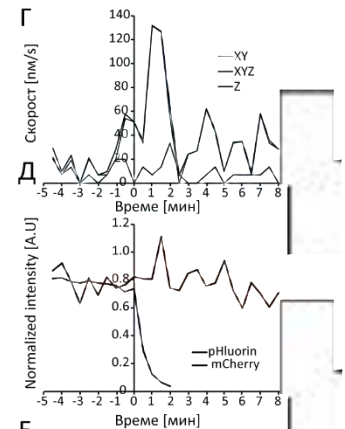
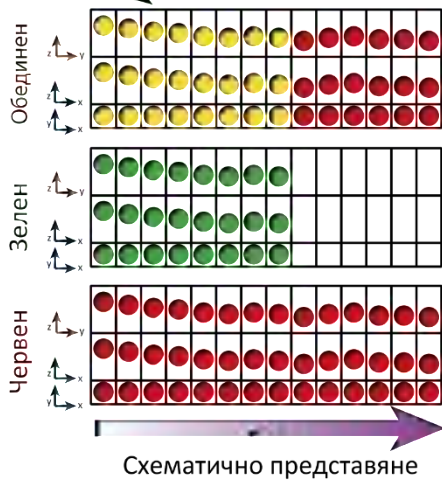
Б

Времева точка 1 (T1)

Времева точка 2 (T2)



В



3.

SPARTACUSS.

3D Gaussian Blur,

3D (),

(mCherry pHluorin).

(maximum intensity $x - z$ y; maximum intensity $y - z$ x; maximum intensity $z - x$ y) (

(), () , ().

(ZY- , ZX- , YX-).

1D- (Z), 2D (XY) 3D (XYZ).

(-M-pHluorin; SARS-CoV-2 -M-mCherry), ().

SPARTACUSS,

(10-20 /),

Z (. 2).

mNeonGreen.

3D.

$VLP^{Wu}:M^{Ch}$,

(. 2).

(. 2).

(. 2).

$VLP^{Wu}:M^{Ch}$,

SPATACUSS,

3D

ACE2

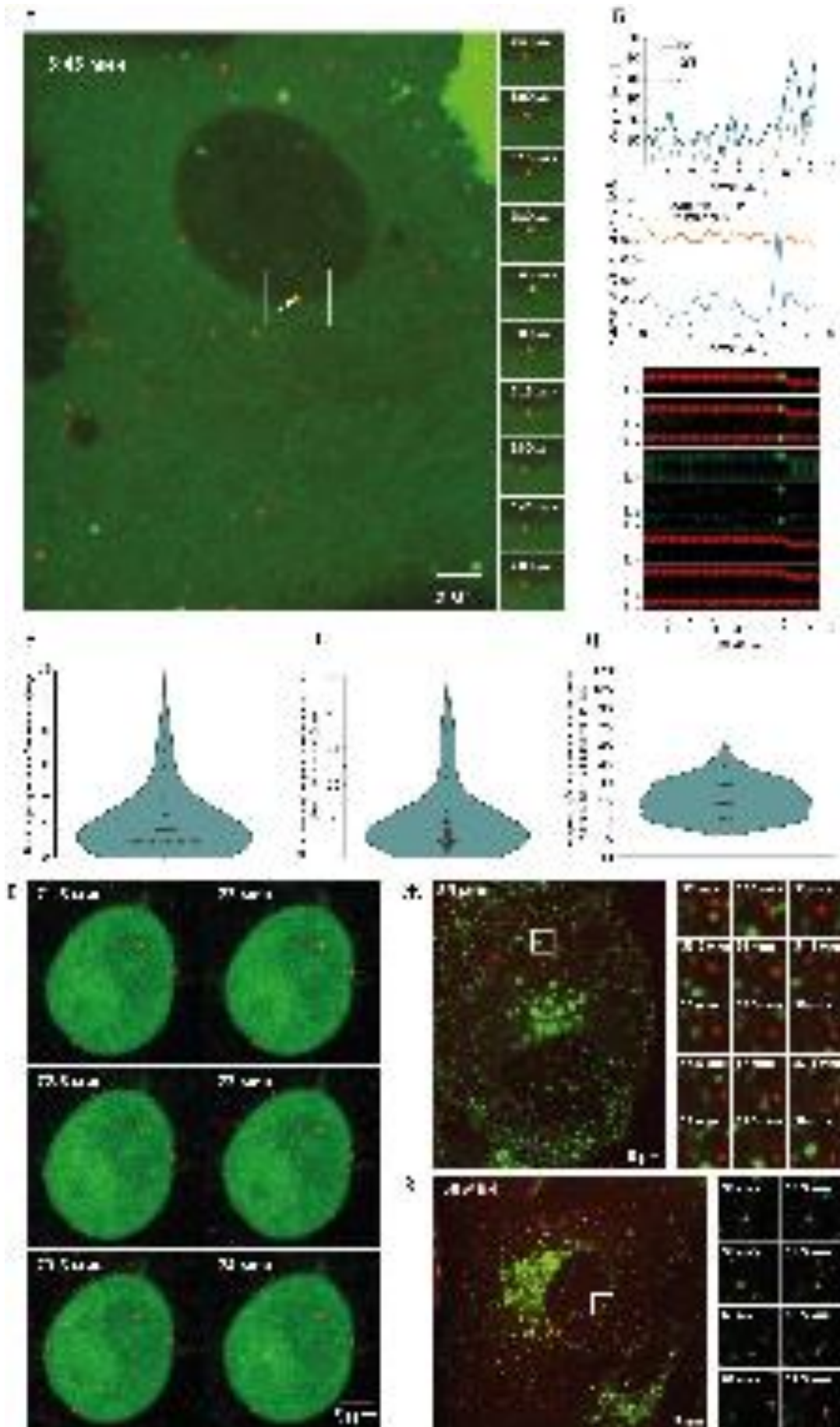
SPARTACUSS

3D

VLP^{Wu}:M^{Ch}.
(cabazitaxel, LIVE 610) 10
, (. 2), ,
SARS-CoV-2
VLP^{Wu}:M^{Ch},
CoV-2 Spike S1 (CR3022 clone) - SARS-CoV-2
- Anti-SARS-
(. 2).

1.2. - -
, 16,17 SARS-
CoV-2 - SARS-
, GFP VeroE6
SARS-CoV-2 ¹⁸.
10-15
()
19-21 , 19,22-24
-1-GFP , VLP^{Wu}:M^{Ch},
() ” “ , 49%
(.

4,).



4.

VLP^{Wu:M^{Ch}} VeroE6

SARS-CoV-2 VLP^{Wu:M^{Ch}},

VeroE6

5:45 ()

();

SARS-

CoV-2 VLP^{Wu:M^{Ch}}, n=41.

, n=37.

VLP^{Wu:M^{Ch}}

. n=18.

E. Dynole 34-2,

Rab-5 GFP.
SARS-CoV-2 VLP^{Wu:M^{Ch}}.
LysoTracker.

Rab-

() ()

()

25.

SPARTACUSS

.4 , 64%

, 17%

, 19%

3

, 36%

()

4).

5.24±6.8

, SPARTACUSS

CoV-2 VLP^{Wu:M^{Ch}}

c

45

30%

(.4 ,)

Dynol 34-2 -

1,

24.

(.4)

, Dynol 34-2

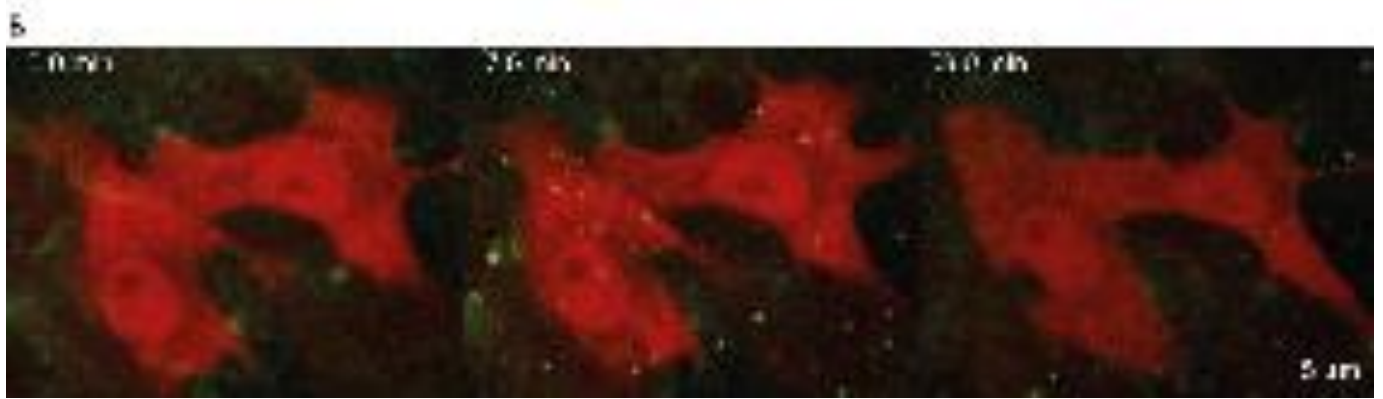
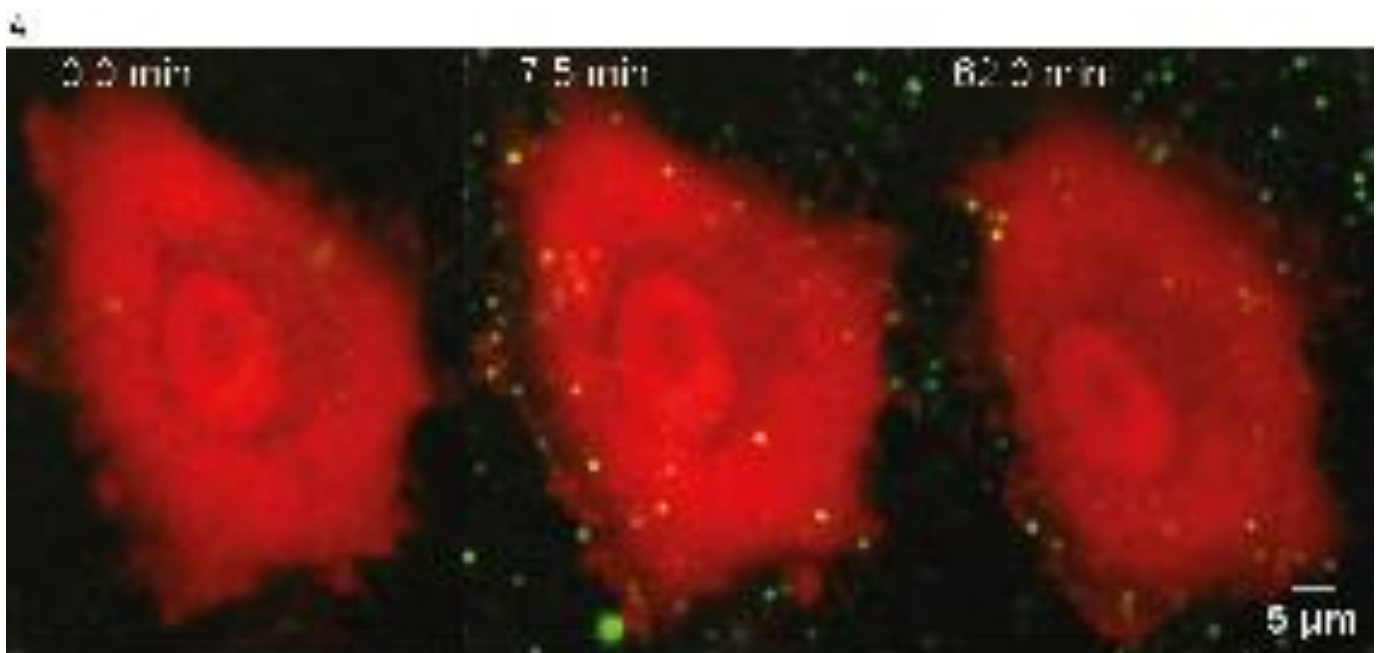
,
 ,
 ,
 Rab-5a GFP ,
 Rab5a-
 - pH (.4).
 ,
 26
 LysoTracker.
 SARS-CoV-2 VLP^{Wu}:M^{Ch} .
 (.4).
 -1-

, Rab-5 .
 SARS-CoV-2
 VLP^{Wu}:M^{Ch}.

1.3.

-
 , pH
 VSV
 SARS-CoV-2 S .
 (fusion), -
 pH SARS-CoV-2 -
 27-29
 M
 pH
 supereclitic pHluorin C 5.
 pH 8,
 pH<7.5, pH<5³⁰. C-
 () -
 pHluorin pH
 - ,
 (pH=8), pHluorin, ,

pH (.5).

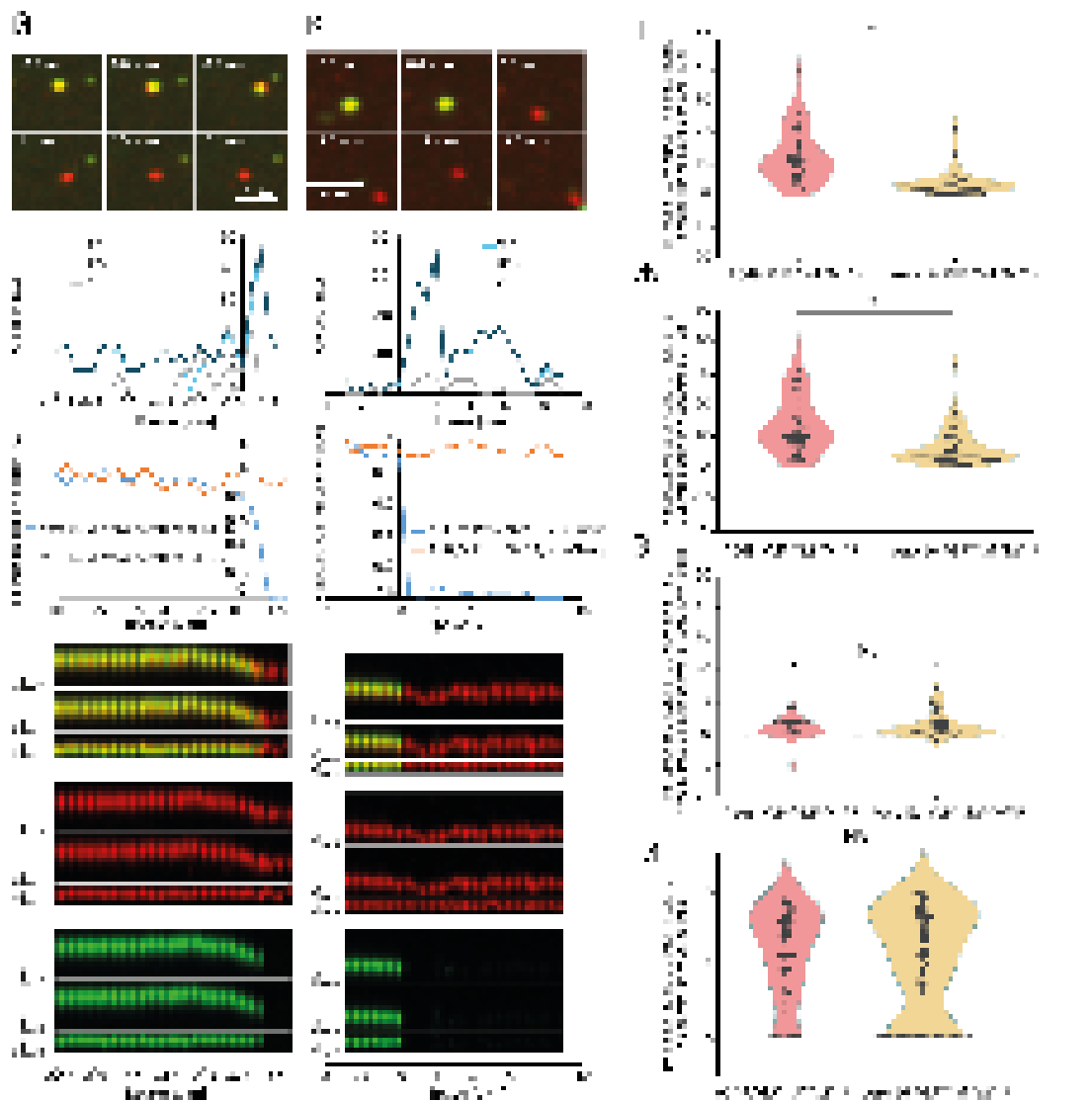
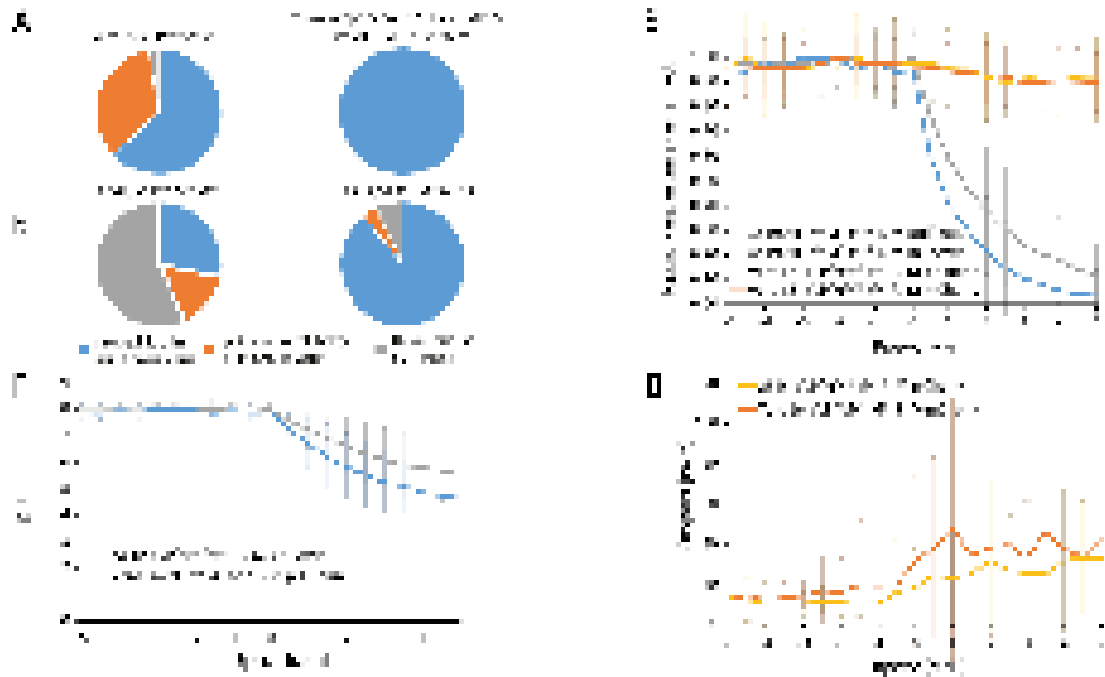


5. pHluorin.

pHluorin 549
 mCherry.
 pHluorin VeroE6
 mCherry.
 pH
 E, S, N M
 pH -mCherry,
 -pHluorin -

31.
 VLP^{Wuhan}:(E, S, N, M&M-mCherry&M-pHluorin).
 VLP^{Wu}:M^{Ch}M^{pH} (
 pHluorin

63% , pH- . ,
 pHluorin
 mCherry, 34%
 3%
 VeroE6 (6). ,
 2/3 pHluorin
 pH .



6.

SARS-CoV-2 VLP^{Wu:M^{Ch}M^{pH}R} 549 pH 6.5

-pHluorin M-mCherry M-pHluorin (),
 VLP^{Wu}:M^{Ch}M^{pHR} VeroE6 () 100 ACE2
 TMPRSS2 (), 549
 VLP^{Wu}:M^{Ch}M^{pHR} 549 VeroE6 M-pHluorin pHluorin
 pHluorin (0).
 M-mCherry (Error Bars) A549 n = 55, a
 VeroE6 n = 93.
 VLP^{Wu}:M^{Ch}M^{pHR} 549 VeroE6 pH M-pHluorin pH pH
 pHluorin (0).
 (Error Bars) A549 n = 55, a
 VeroE6 n = 93.
 VLP^{Wu}:M^{Ch}M^{pHR}, 549 VeroE6 pHluorin (0).
 (Error Bars) A549 n = 55, a
 VeroE6 n = 93.
 VLP^{Wu}:M^{Ch}M^{pHR} 549 VeroE6 pHluorin : NS p>0.01; *
 t- A549 n = 55, a VeroE6 n = 93.
 VLP^{Wu}:M^{Ch}M^{pHR} 549 VeroE6 t- : NS p>0.01; * p<0.01. A549 n = 55,
 a VeroE6 n = 93.
 pHluorin VLP^{Wu}:M^{Ch}M^{pHR} 549 VeroE6 : NS
 t- A549 n = 55, a VeroE6 n = 93.
 p>0.01; * p<0.01. pH VLP^{Wu}:M^{Ch}M^{pHR}, pHluorin 549 VeroE6 : NS
 t- A549 n = 55, a VeroE6 n = 93.
 (),
 (-) (),
 M-mCherry M-pHluorin VeroE6 ,
 VLP^{Wu}:M^{Ch}M^{pHR} pHluorin ,
 (), A549 .

- TMPRSS2.
 (VLP^{Wu}:M^{Ch}M^{pH}, R), - 20 - 31.

mCherry. pHluorin
 ACE2 TMPRSS2
 (100%).
 549 SARS-CoV-2.

ACE2 TMPRSS2 28% pHluorin
 mCherry. 15% -
 57%
 (. 6).

A549 - SARS-CoV-2 -
 VeroE6 ACE2 TMPRSS2
 pHluorin
 mCherry (89% 28%).
 ACE2 TMPRSS2 ,

pH,
 (. 6). pHluorin ,

(. 6).
 pHluorin, 1.4 1.6 a VeroE6 A549
 pHluorin pH
 A549 8 6.9 90 (. 6), pH 8 6.3,

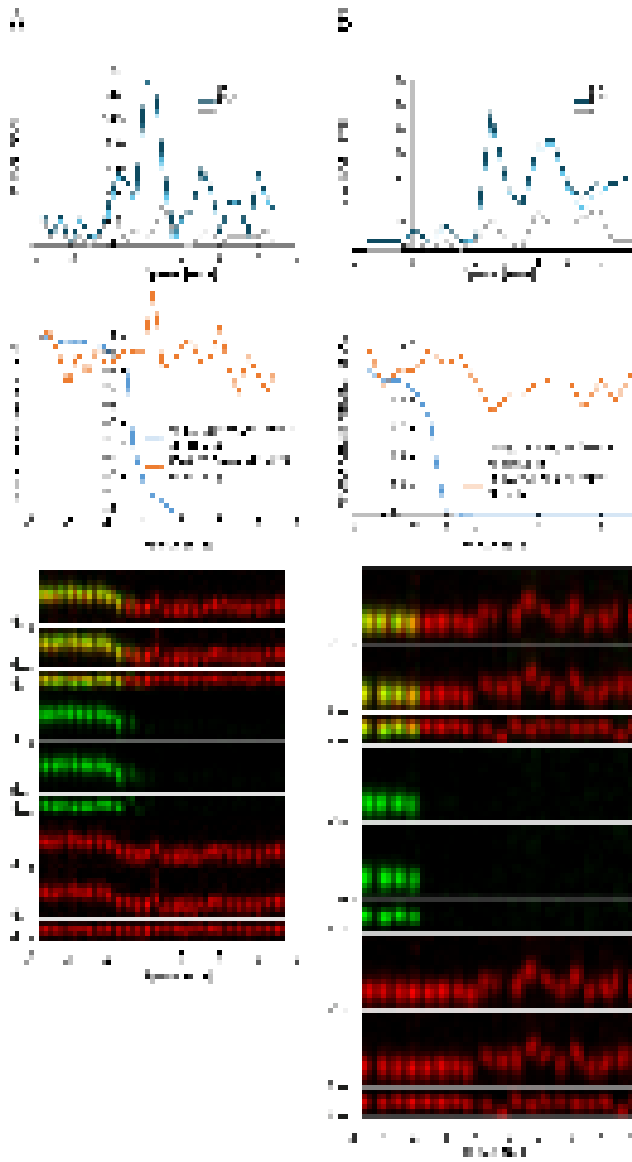
pH (. 6).
 (M-mCherry M-pHluorin) -
 :
 pH

(0.6 , , , , 1).

		pHluorin EGFP	N-	
VLP-WT VeroE6	MM	4.1 ± 3.6 min	2.4 ± 3.7 min	6.5 ± 5.4 min
VLP-WT	MM A549	12.5 ± 8.4 min	1.4 ± 3.7 min	13.9 ± 9.2 min
VLP-WT	NM A549	13 ± 8.6 min	7.0 ± 10.0 min	20.1 ± 14.8 min
VLP-Omi	NM A549	14.2 ± 8.5 min	2.9 ± 6.9 min	17.1±10.1 min
VLP-del1 VeroE6	MM	6.4 ± 5.4 min	2.8 ± 8.2 min	9.2 ± 8.9 min
VLP-del1 A549	MM	16.7 ± 12.7 min	1.7 ± 1.6 min	18.4 ± 12.9 min
VLP-del1 A549	MM	10.12 ± 8.72 min	3.61 ± 7.79 min	13.74 ± 11.57 min
VLP-OMI A549	MM	13.01 ± 8.4 min	4.03 ± 7.44 min	17.04 ± 11.48 min

1.

VeroE6 , pH 4.1 ± 3.6
 , 2.4 ± 3.7
 (1). 549 pH 12.5
 ± 8.4 , 1.4 ± 3.7
 , pH
 (0.6 ,).
 pH (0.7 8),



7.

pHluorin)

()

pHluorin

(),

pHluorin

(

5

()

(, M-Cherry

M-

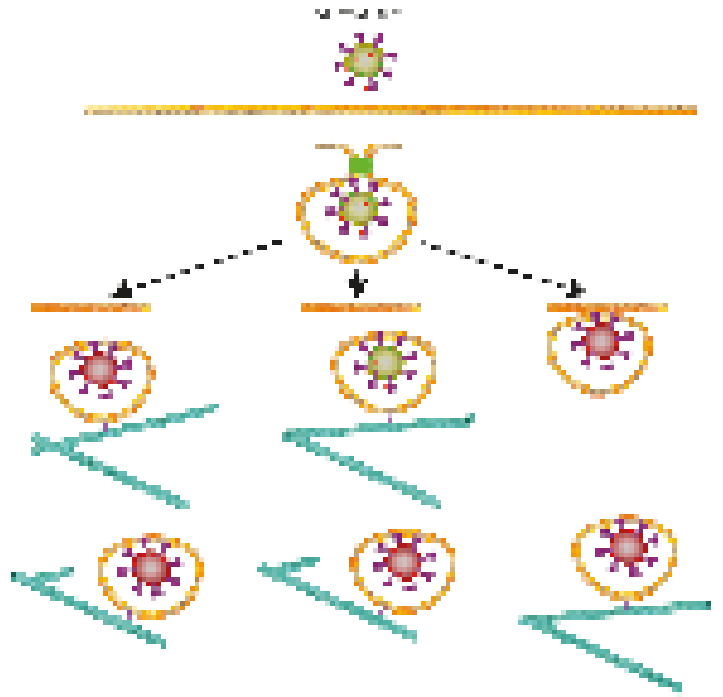
(). pH
(); pH

(); pH
()

5

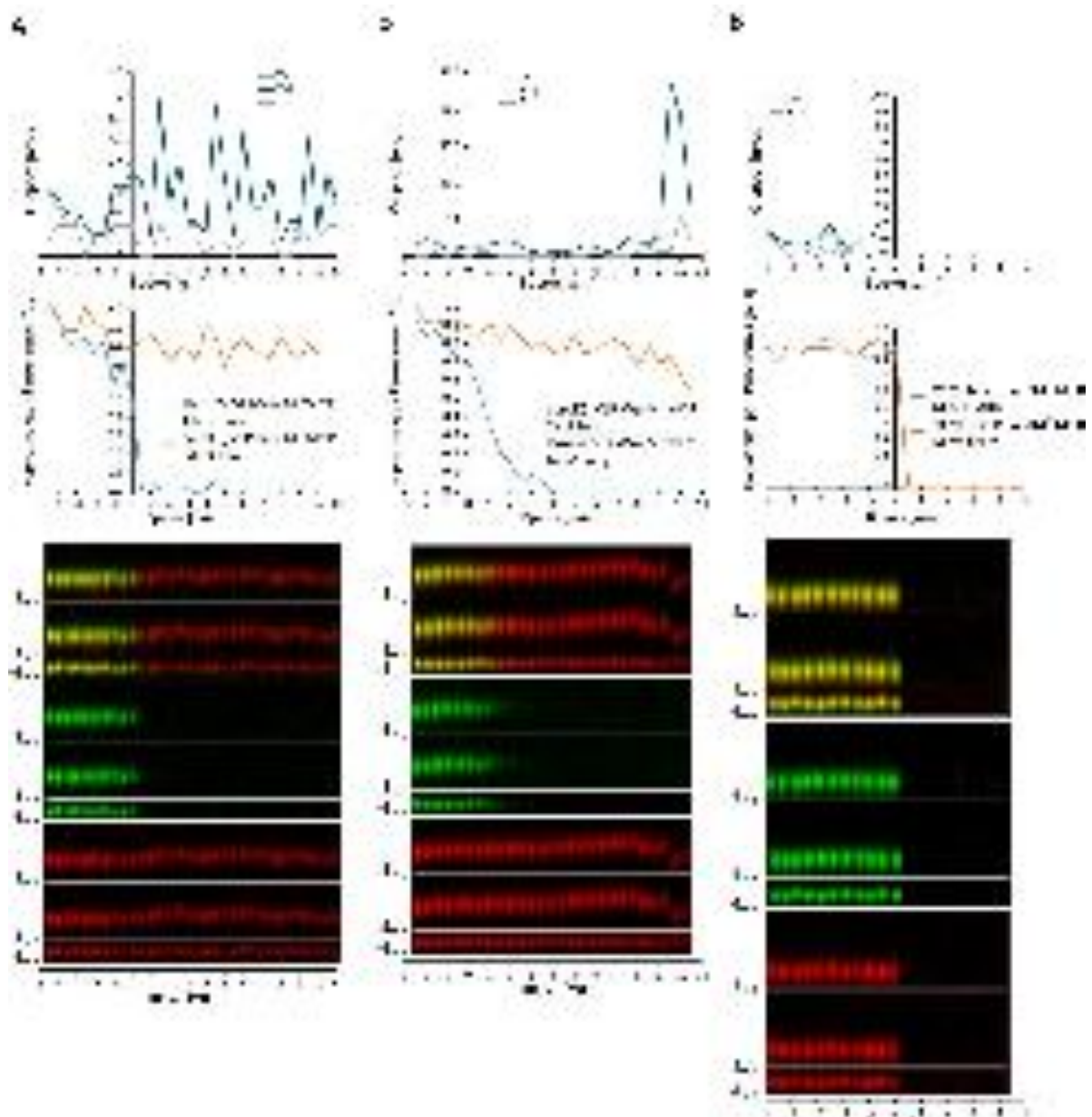
).

8



VLP^{Wu}:M^{Ch}M^{pHR}

549



8.

VLP^{Wu}:M^{Ch}M^{pHR} VeroE6

pHluorin) () () () , M-Cherry M-
 pHluorin () ,
 pHluorin () ,

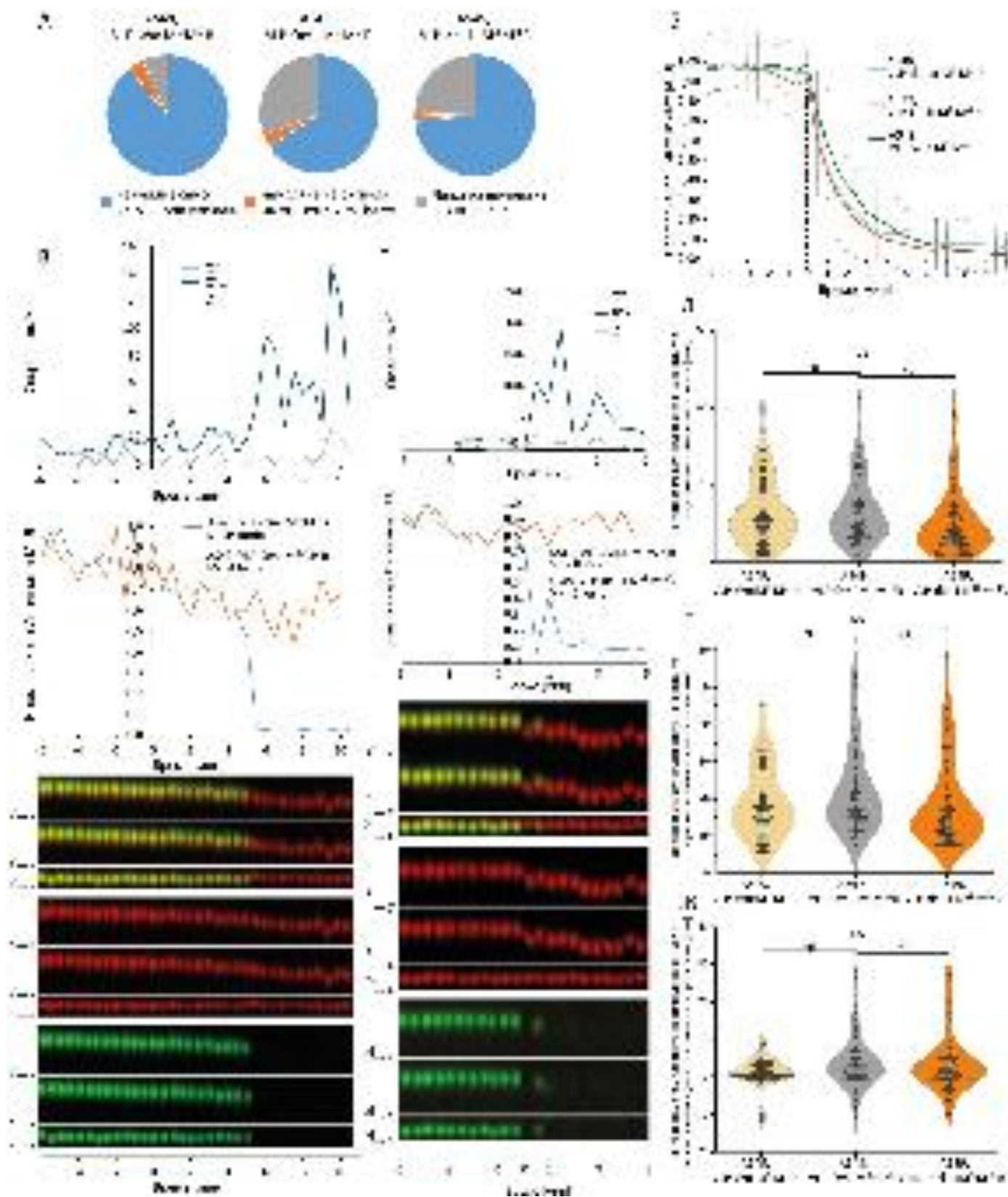
(pH)
 (. 6).
 (. 7).
 pH <5.
 (. 6)
 pH ()
 () 2 3
 VeroE6 A549 (. 6) 1).
 VeroE6 549 SARS-CoV-2 .
 pH-
 549 (. 6 ,).
 VeroE6 549 .
 :
 ,

1.4.

Furin

SARS-CoV SARS-CoV-2,
 (PRRA)

S1 S2 S , Furin ³².
 Furin, S2' TMPRSS2
 , S - .
 , (FCS)
 SARS-CoV-2 - M-mCherry, M-pHluorin S ,
 FCS (del-1) ³³⁻³⁷.
 VLP^{Wu(del-1)}:M^{Ch}M^{pH},R; VLP^{Wuhan(del-1)}:(N, E, S, M&M-mCherry & M-pHluorin,
 T20 RNA). 549 , ACE2 TMPRSS2
 VLP^{Wu(del-1)}:M^{Ch}M^{pH},R, pHluorin
 mCherry - 89% VLP^{Wu}:M^{Ch}M^{pH},R
 73% VLP^{Wu(del-1)}:M^{Ch}M^{pH}, R (. 9).
 pHluorin - (. 9).
 pH
 (. 9 - , 1). ,
 , pH
 (.10). , -



9.

VLP^{Wu}: M^{Ch}M^{pH}R, VLP^{Omi}: M^{Ch}M^{pH}R and VLP^{Del-1}: M^{Ch}M^{pH}R

549

), M-pHluorin (), M-mCherry ().

pHluorin : VLP^{Wu}: M^{Ch}M^{pHR}, 549 .

VLP^{Omi}: M^{Ch}M^{pHR} and VLP^{del-1}: M^{Ch}M^{pHR} pHluorin , -pHluorin (0).

(Error Bars) VLP^{Wu}: M^{Ch}M^{pHR} .

n=55, VLP^{Omi}: M^{Ch}M^{pHR} n=48 VLP^{del-1}: M^{Ch}M^{pHR} n=62. ()

(, M-mCherry M-pHluorin) ()

VLP^{Omi}: M^{Ch}M^{pHR} - 549 .

-pHluorin VLP^{del-1}: M^{Ch}M^{pHR}. -

-pHluorin VLP^{Wu}: M^{Ch}M^{pHR}, VLP^{Omi}: M^{Ch}M^{pHR} VLP^{del-1}: M^{Ch}M^{pHR}. t-

M^{Ch}M^{pHR}, 549 . : NS p>0.01; * p<0.01 VLP^{Wu}: M^{Ch}M^{pHR} n=55, VLP^{Omi}: M^{Ch}M^{pHR} n=48 VLP^{del-1}: M^{Ch}M^{pHR} n=62. -

549 . : VLP^{Wu}: M^{Ch}M^{pHR}, VLP^{Omi}: M^{Ch}M^{pHR} VLP^{del-1}: M^{Ch}M^{pHR}. t- : NS

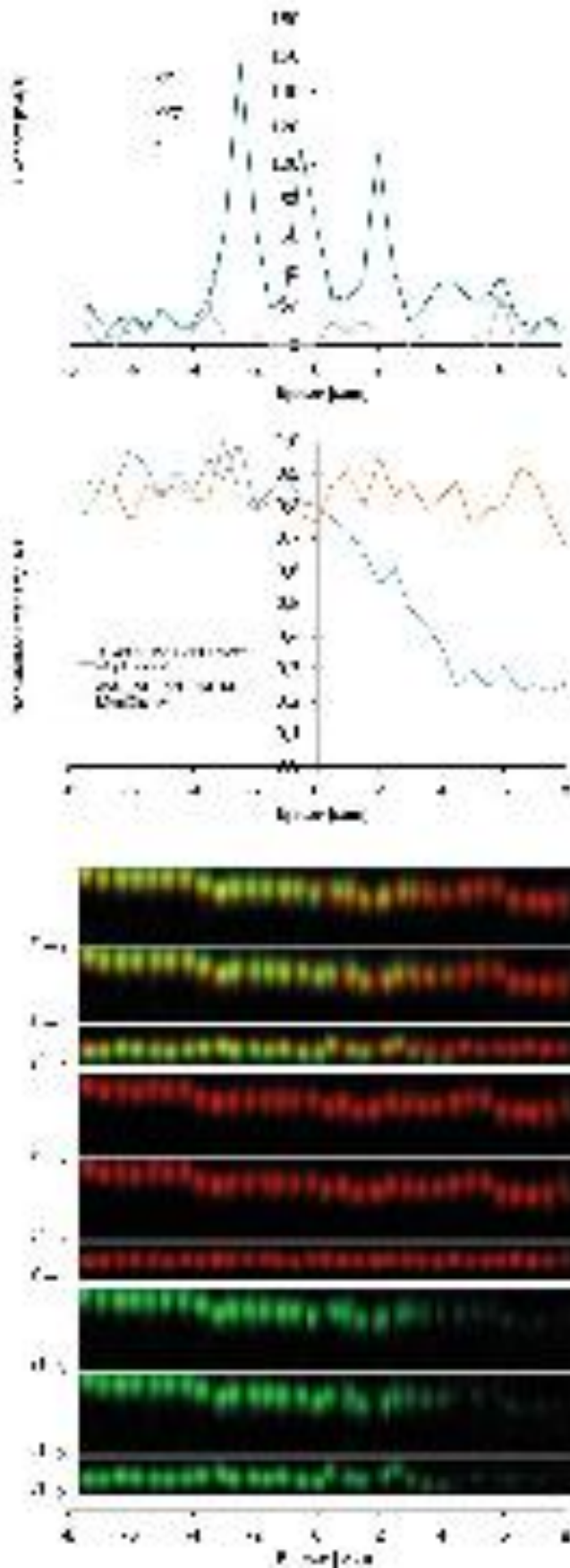
p>0.01; * p<0.01 VLP^{Wu}: M^{Ch}M^{pHR} n=55, VLP^{Omi}: M^{Ch}M^{pHR} n=48 VLP^{del-1}: M^{Ch}M^{pHR} n=62. -

pHluorin - M- 549 . : VLP^{Wu}: M^{Ch}M^{pHR}, VLP^{Omi}: M^{Ch}M^{pHR}

VLP^{del-1}: M^{Ch}M^{pHR}. t- : NS p>0.01; * p<0.01 VLP^{Wu}: M^{Ch}M^{pHR} n=55, VLP^{Omi}: M^{Ch}M^{pHR} n=48

VLP^{del-1}: M^{Ch}M^{pHR} n=62.

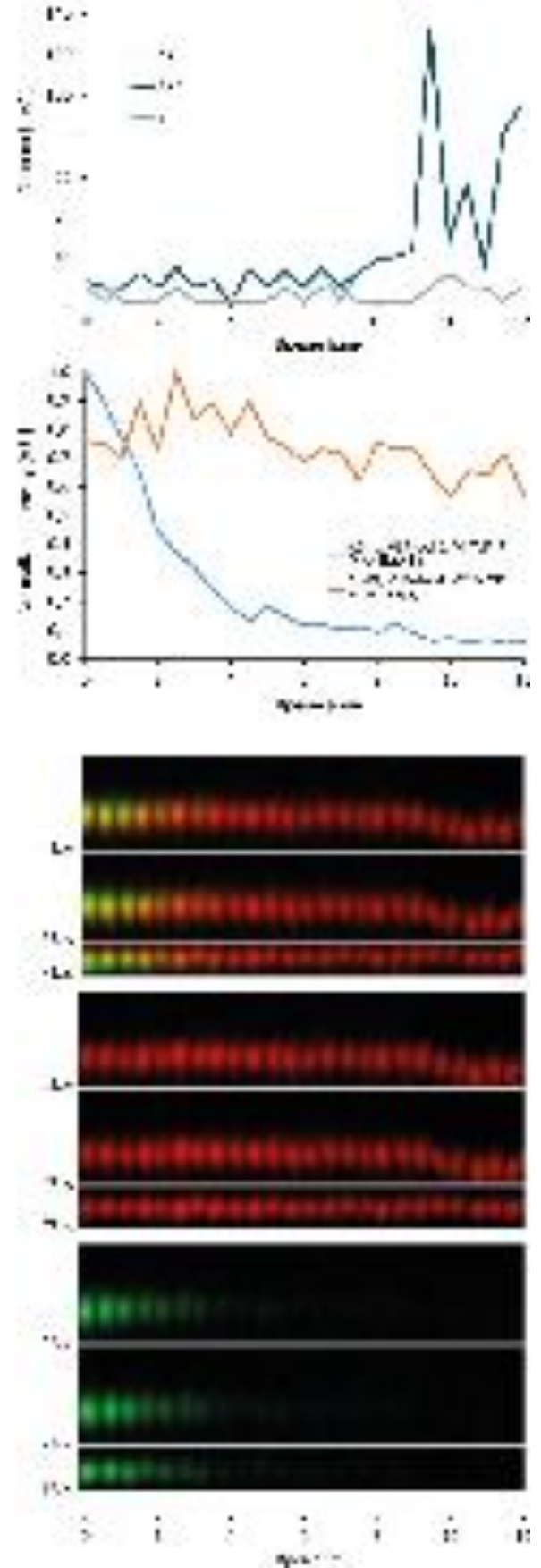
A



10.

VLP^{del-1}:M^{Ch}M^{PHR}.

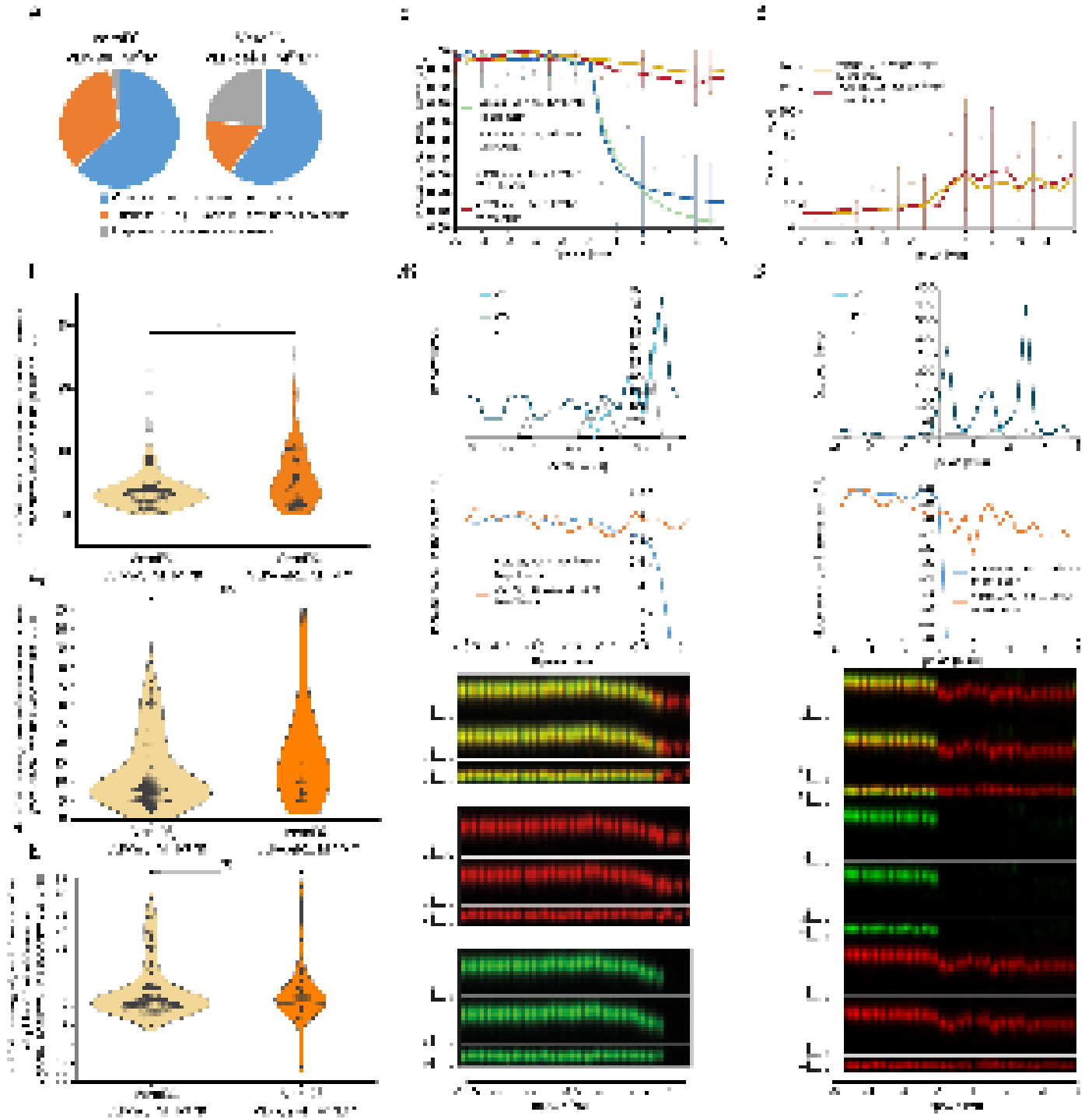
B



549

pHluorin) () () () , M-Cherry M-
,
pHluorin
(),
pHluorin

VeroE6 (.11 12).



11.

VLP^{Wu}:M^{Ch}M^{pH} and VLP^{del-1}:M^{Ch}M^{pH}
VeroE6

), M-pHluorin (M-mCherry (M-pHluorin (

$VLP^{del-1}:M^{Ch}M^{pHR}$, pHluorin
 M-mCherry
 (Error Bars)
 VeroE6- $VLP^{del-1}:M^{Ch}M^{pH}$ n=41.

pHluorin : $VLP^{Wu}:M^{Ch}M^{pHR}$
 549
 -pHluorin (0).
 VeroE6- $VLP^{Wu}:M^{Ch}M^{pHR}$ n=93,

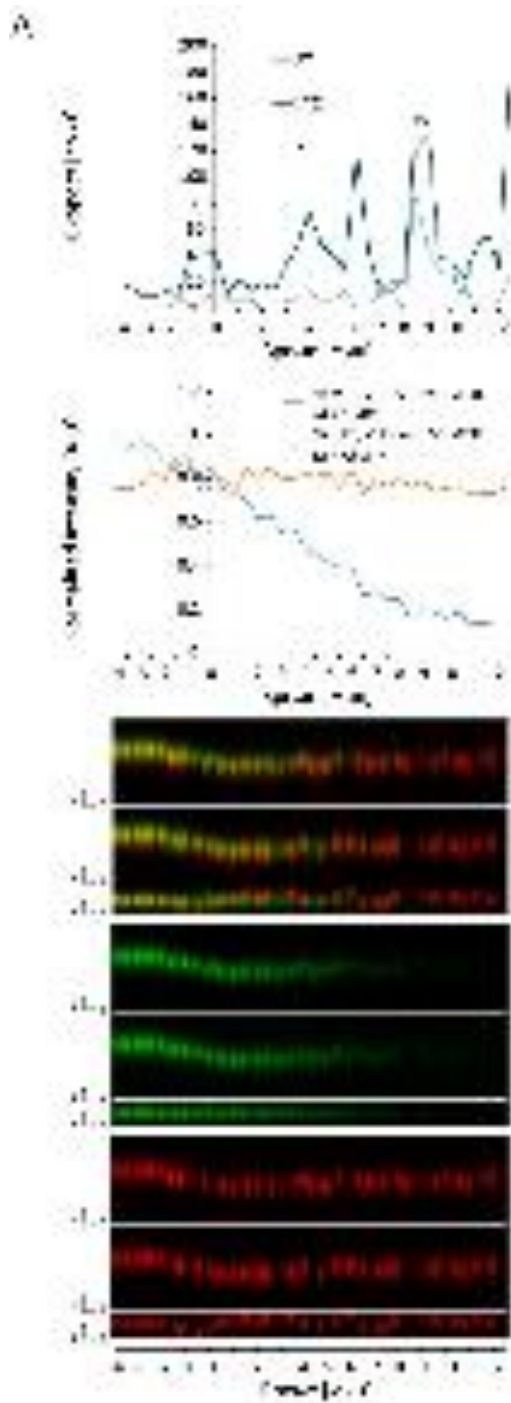
$VLP^{Wu}:M^{Ch}M^{pH}$ and $VLP^{del-1}:M^{Ch}M^{pH}$ VeroE6
 pHluorin (0).
 (Error Bars) VeroE6- $VLP^{Wu}:M^{Ch}M^{pHR}$
 n=93, VeroE6- $VLP^{del-1}:M^{Ch}M^{pH}$ n=41.

-pHluorin
 $VLP^{Wu}:M^{Ch}M^{pH}$ $VLP^{del-1}:M^{Ch}M^{pH}$,
 VeroE6 t-
 : NS p>0.01; * p<0.01 VeroE6- $VLP^{Wu}:M^{Ch}M^{pHR}$
 n=93, VeroE6- $VLP^{del-1}:M^{Ch}M^{pH}$ n=41.

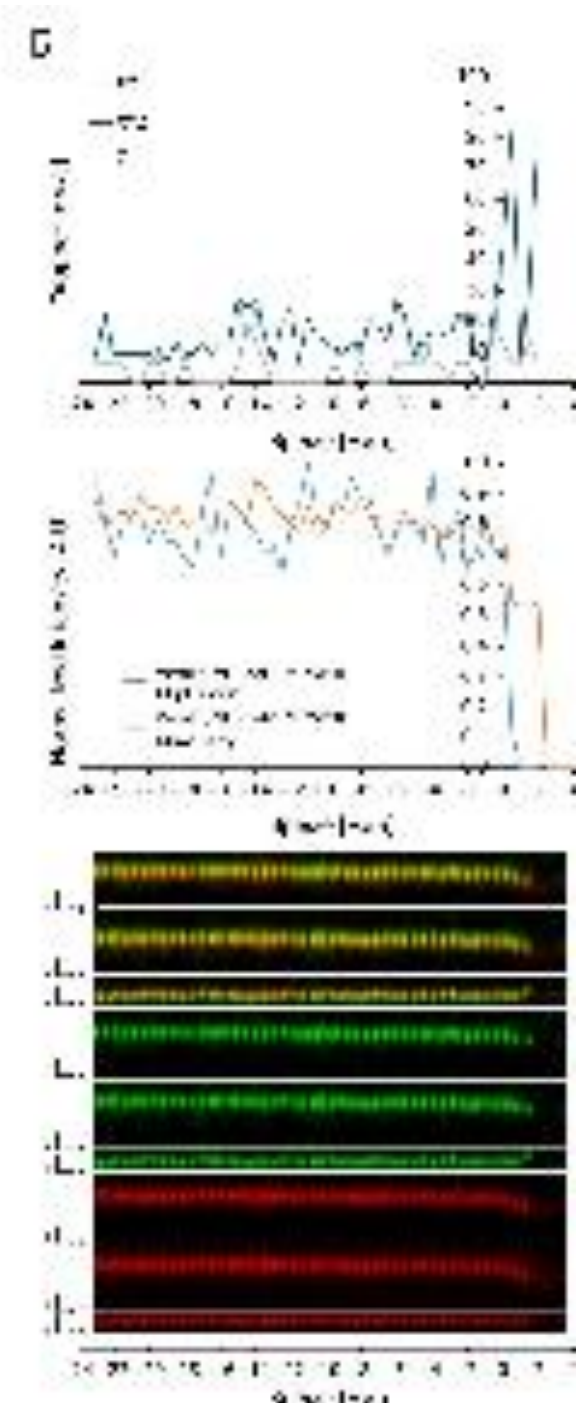
VeroE6 : $VLP^{Wu}:M^{Ch}M^{pH}$ $VLP^{del-1}:M^{Ch}M^{pH}$.
 t- : NS p>0.01; *
 p<0.01 VeroE6- $VLP^{Wu}:M^{Ch}M^{pHR}$ n=93, VeroE6- $VLP^{del-1}:M^{Ch}M^{pH}$ n=41.

M-
 pHluorin -
 VeroE6 : $VLP^{Wu}:M^{Ch}M^{pH}$ $VLP^{del-1}:M^{Ch}M^{pH}$.
 t- : NS
 p>0.01; * p<0.01 VeroE6- $VLP^{Wu}:M^{Ch}M^{pHR}$ n=93, VeroE6- $VLP^{del-1}:M^{Ch}M^{pH}$ n=41.

(-) (),
 () VeroE6
 M-mCherry M-pHluorin
 $VLP^{Wu}:M^{Ch}M^{pH}$ - VeroE6
 pHluorin (), - $VLP^{del-1}:M^{Ch}M^{pHR}$.



12.



VLP^{del-1}:M^{Ch}M^{pH} VeroE6

pHluorin) () () () , M-Cherry M-
 pHluorin () ,

SARS-CoV-2 - , FCS , SARS-

CoV-2 VeroE6 S1 S2

37,38 , FCS

- FCS, Furin

1.5. - ,

SARS-CoV-2

SARS-CoV-2 2021 .

15 50 - , 37, S ,

39,40 , 39 ,

70 - , N, E, S

- , mCherry pHluorin

VLP^{Omicron}:(N, E, S, M, M-mCherry & M-pHluorin, T20 RNA). VLP^{Omi}:M^{Ch}M^{pHR},

549 , ACE2 TMPRSS2, ,

pHluorin

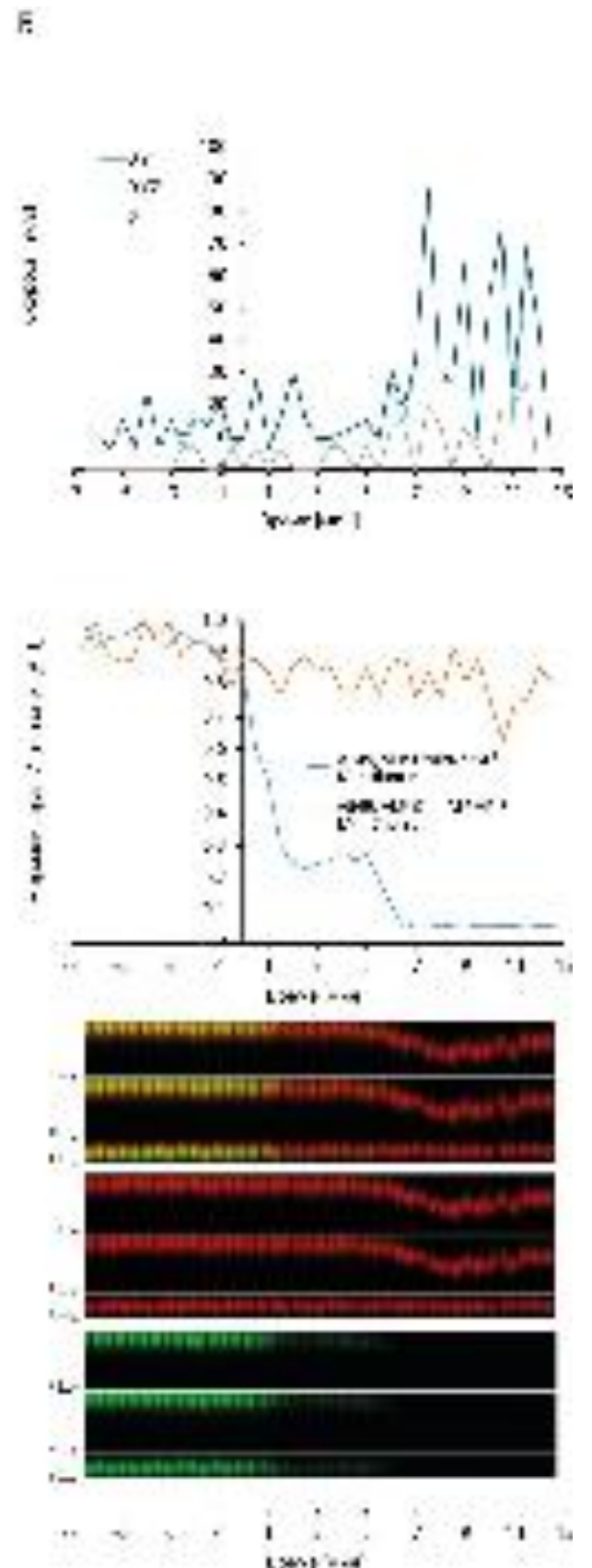
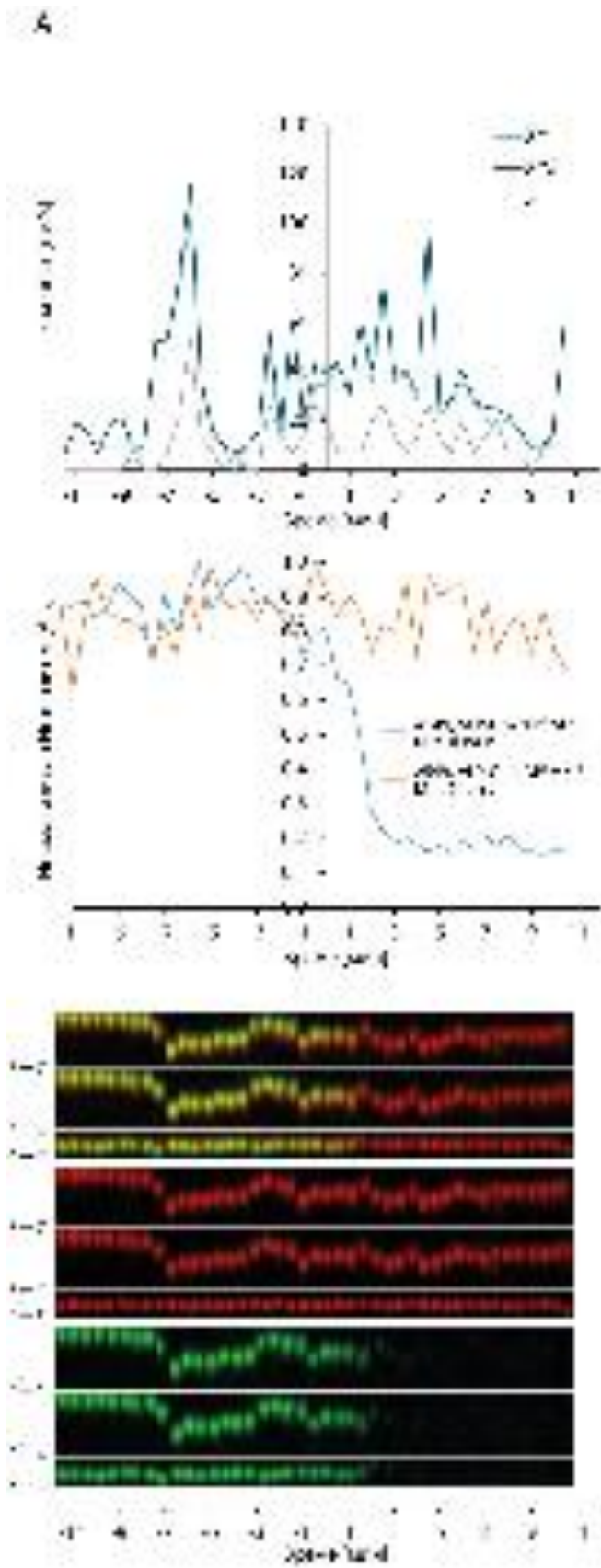
mCherry - 89% VLP^{Wu}:M^{Ch}M^{pHR} 65% VLP^{Omi}:M^{Ch}M^{pHR}

(.9). pHluorin

(.9).

9 , ,). - (.

pHluorin (.13)



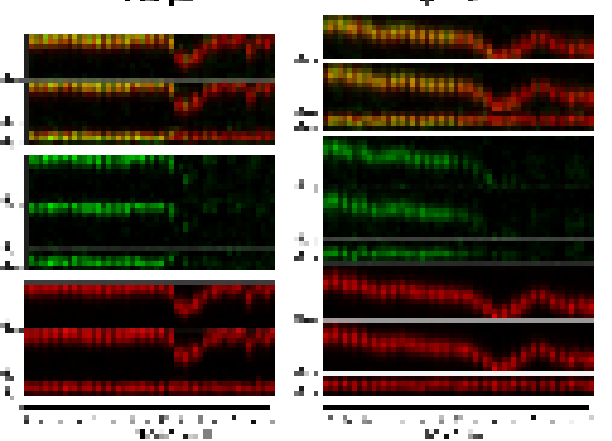
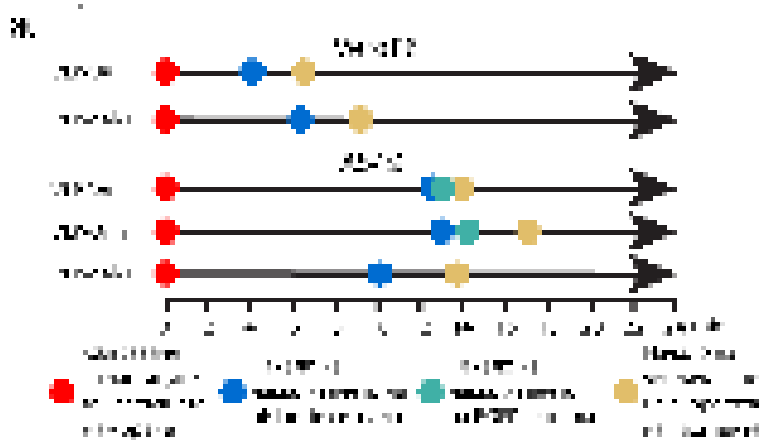
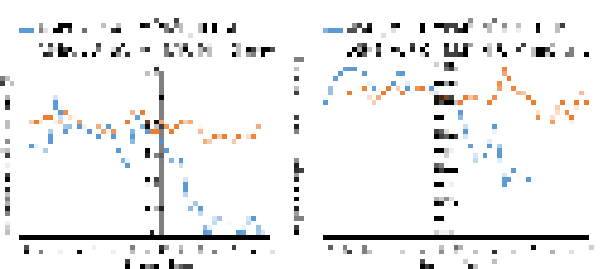
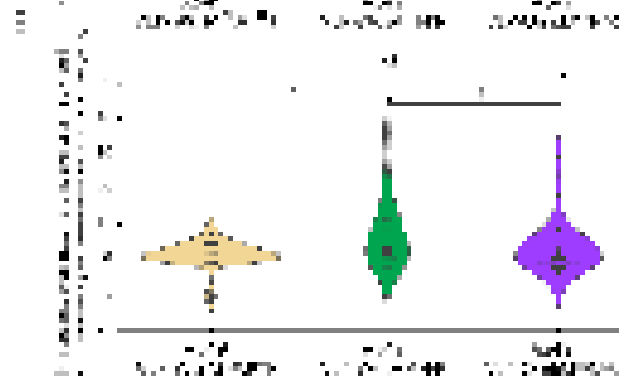
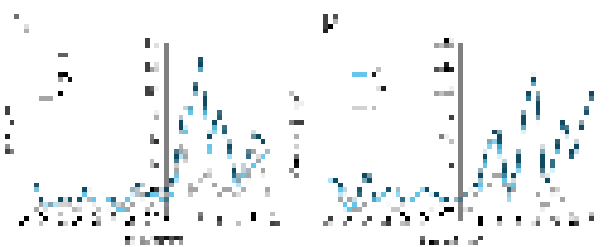
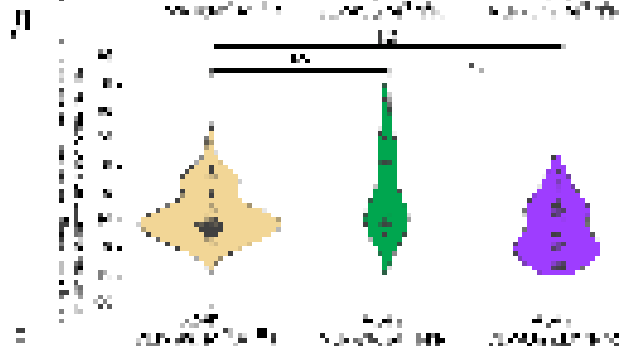
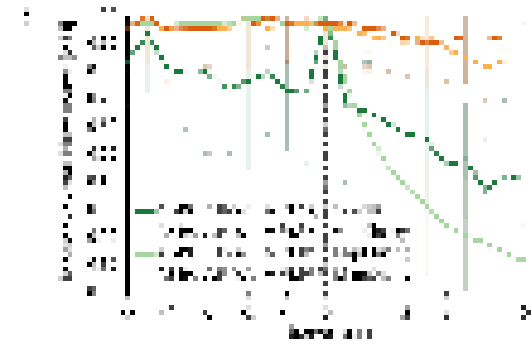
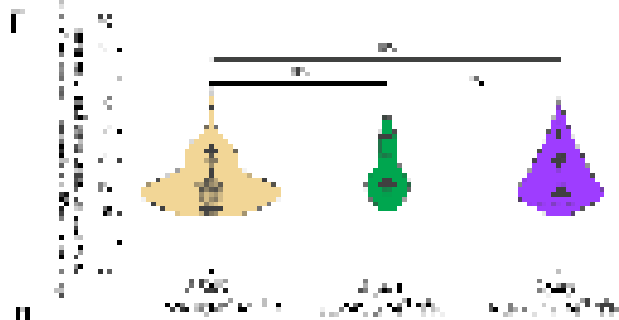
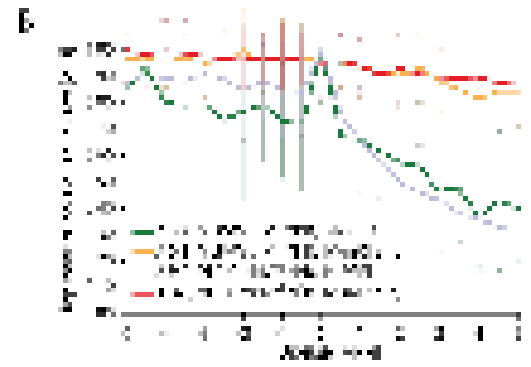
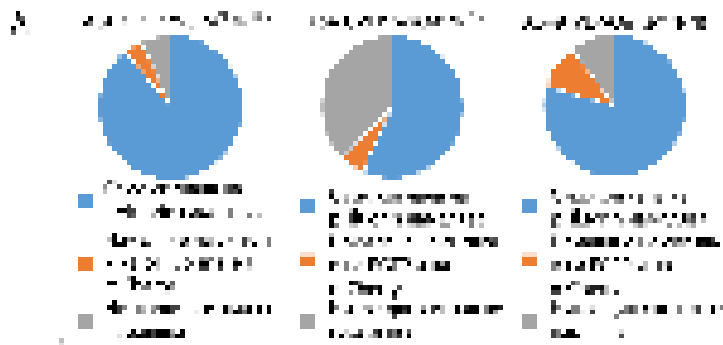
549 13.

VLP^{Omi}:M^{ChM}pH^R

A. pHluorin) () () () , M-Cherry M-
 () ,
 pHluorin ,
 () ,
 pHluorin M- .
 , S

1.6.

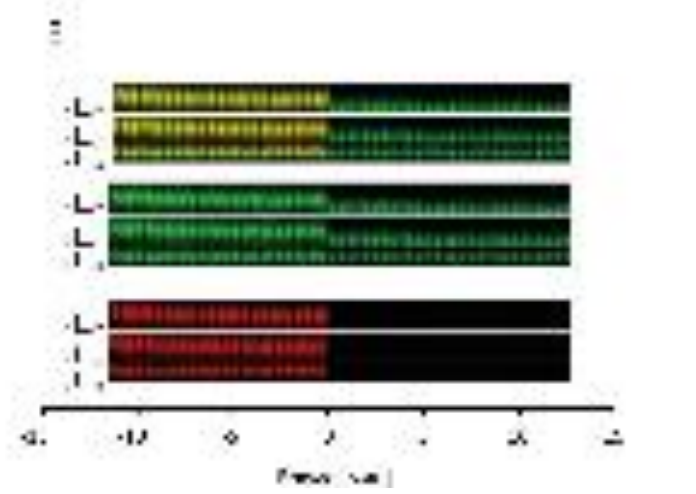
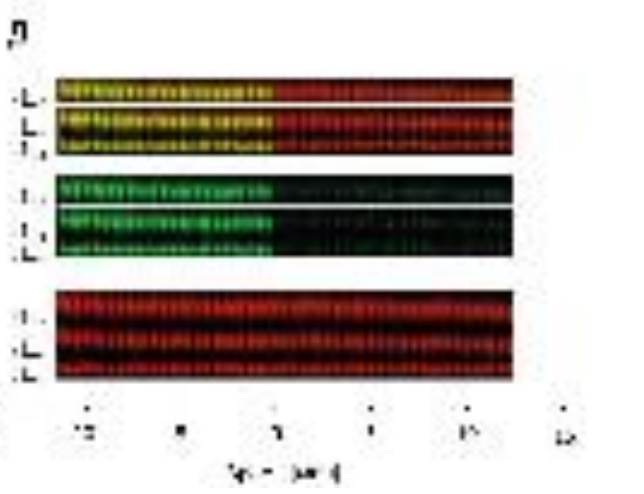
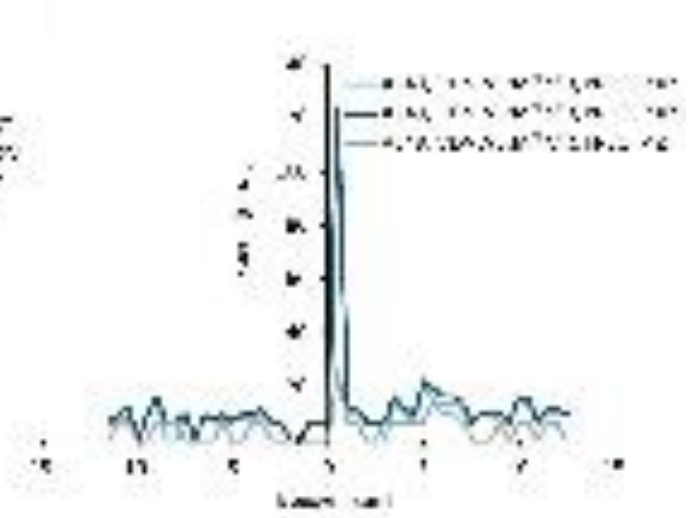
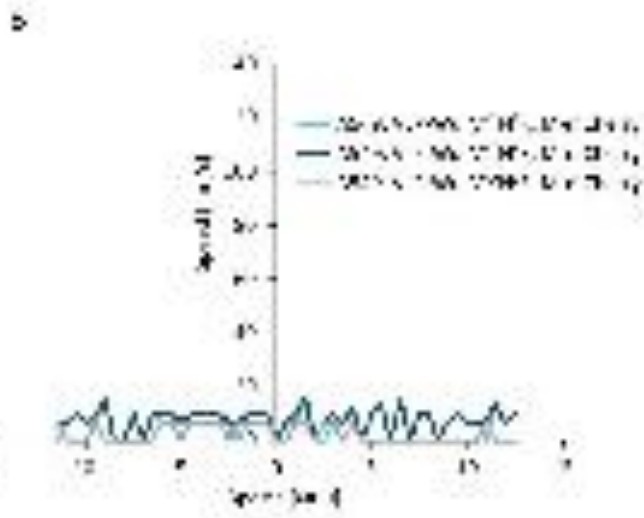
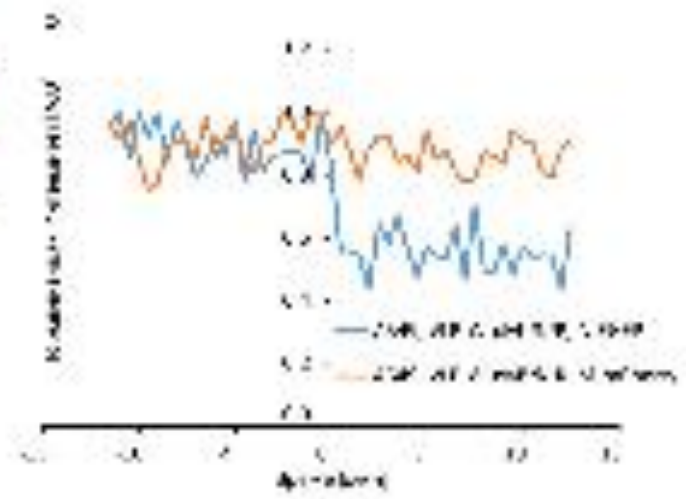
,
 ,
 -
 , N , EGFP, -
 mCherry.
 (VLP^{Wu}:N^{eG}M^{ChR}), SARS-CoV-2:(E, S, N&N-eGFP, M&M-mCherry, T20
 RNA). , , 90%
 1% , -
 , , N
 31 .
 , 57% -
 EGFP
 mCherry, - N (.14).



VLP^{Omi}:M^{ChN^ER}, VLP^{Wu}:M^{ChN^ER}, VLP^{Wu}:M^{ChM^pH^R}
549

M-pHluorin/N-EGFP (), M-pHluorin (), M-mCherry (), N-EGFP (),
 VLP^{Wu}:M^{ChN^ER} EGFP N-EGFP : VLP^{Omi}:M^{ChN^ER} 549
 M-mCherry N-EGFP (0).
 (Error Bars) VLP^{Wu}:M^{ChN^ER} n=17,
 VLP^{Omi}:M^{ChN^ER} n=34. N-EGFP M-pHluorin :
 VLP^{Wu}:M^{ChM^pH^R} VLP^{Wu}:M^{ChN^ER} EGFP pHluorin 549
 N-EGFP pHluorin (0). M-mCherry
 (Error Bars) VLP^{Wu}:M^{ChM^pH^R} n=55, A549 VLP^{Wu}:M^{ChN^ER} n=17.
 -pHluorin N-EGFP
 VLP^{Wu}:M^{ChM^pH^R}, VLP^{Wu}:M^{ChN^ER},
 VLP^{Omi}:M^{ChN^ER}, 549 t-
 : NS p>0.01; * p<0.01
 VLP^{Wu}:M^{ChN^ER} n=17, for VLP^{Omi}:M^{ChN^ER} n=34 and VLP^{Wu}:M^{ChM^pH^R} n=55.
 549 : VLP^{Wu}:M^{ChM^pH^R}, VLP^{Wu}:M^{ChN^ER} VLP^{Omi}:M^{ChN^ER}.
 t- : NS
 p>0.01; * p<0.01 VLP^{Wu}:M^{ChN^ER} n=17, VLP^{Omi}:M^{ChN^ER} n=34 VLP^{Wu}:M^{ChM^pH^R} n=55.
 M-
 pHluorin N-EGFP -
 A549 : VLP^{Wu}:M^{ChM^pH^R}, VLP^{Wu}:M^{ChN^ER}
 VLP^{Omi}:M^{ChN^ER}. t-
 : NS p>0.01; * p<0.01 VLP^{Wu}:M^{ChN^ER} n=17, VLP^{Omi}:M^{ChN^ER} n=34
 VLP^{Wu}:M^{ChM^pH^R} n=55.
 VeroE6 549
 ()
 (, M-mCherry N-EGFP) ()
 VLP^{Wu}:M^{ChN^ER} 549 N-EGFP
 () VLP^{Omi}:M^{ChN^ER}.
 N-EGFP VLP^{Wu}:N^{eG}M^{ChR} -
 M-pHluorin VLP^{Wu}:M^{ChM^pH^R} (. 14) -

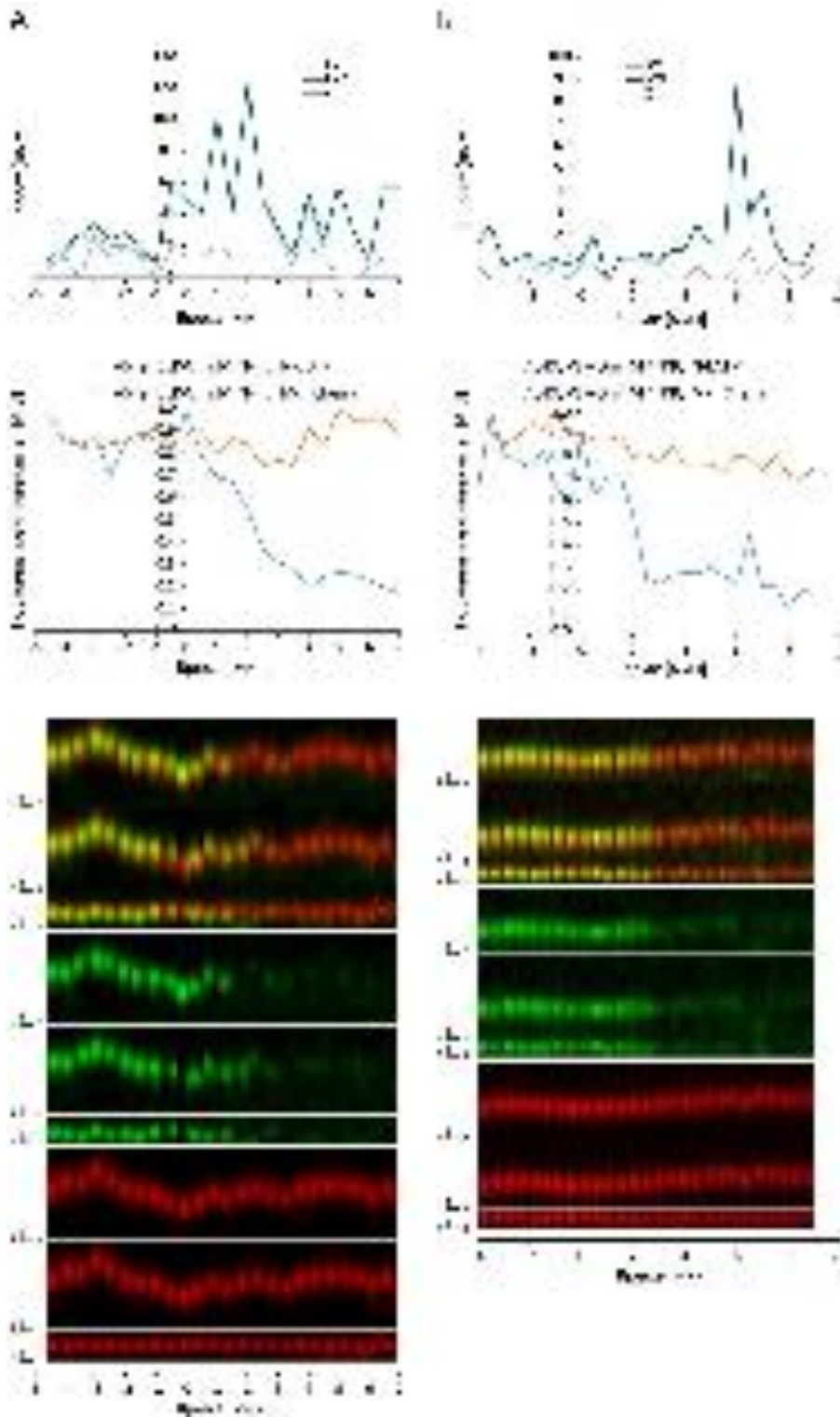
EGFP , , (18 -) N-EGFP (M-mCherry N-EGFP) , M-mCherry , N-EGFP Z , (. 15). , , M-pHluorin VLP^{Wu}:M^{Ch}M^{pHR} (1) N-EGFP VLP^{Wu}:N^{eG}M^{Ch}R (. 14 , ,) .



15.

$VLP^{Wu}:MChN^{ER} \quad 549$
 (N-EGFP) N-EGFP M-mCherry (M-mCherry)
 (), (), M-mCherry

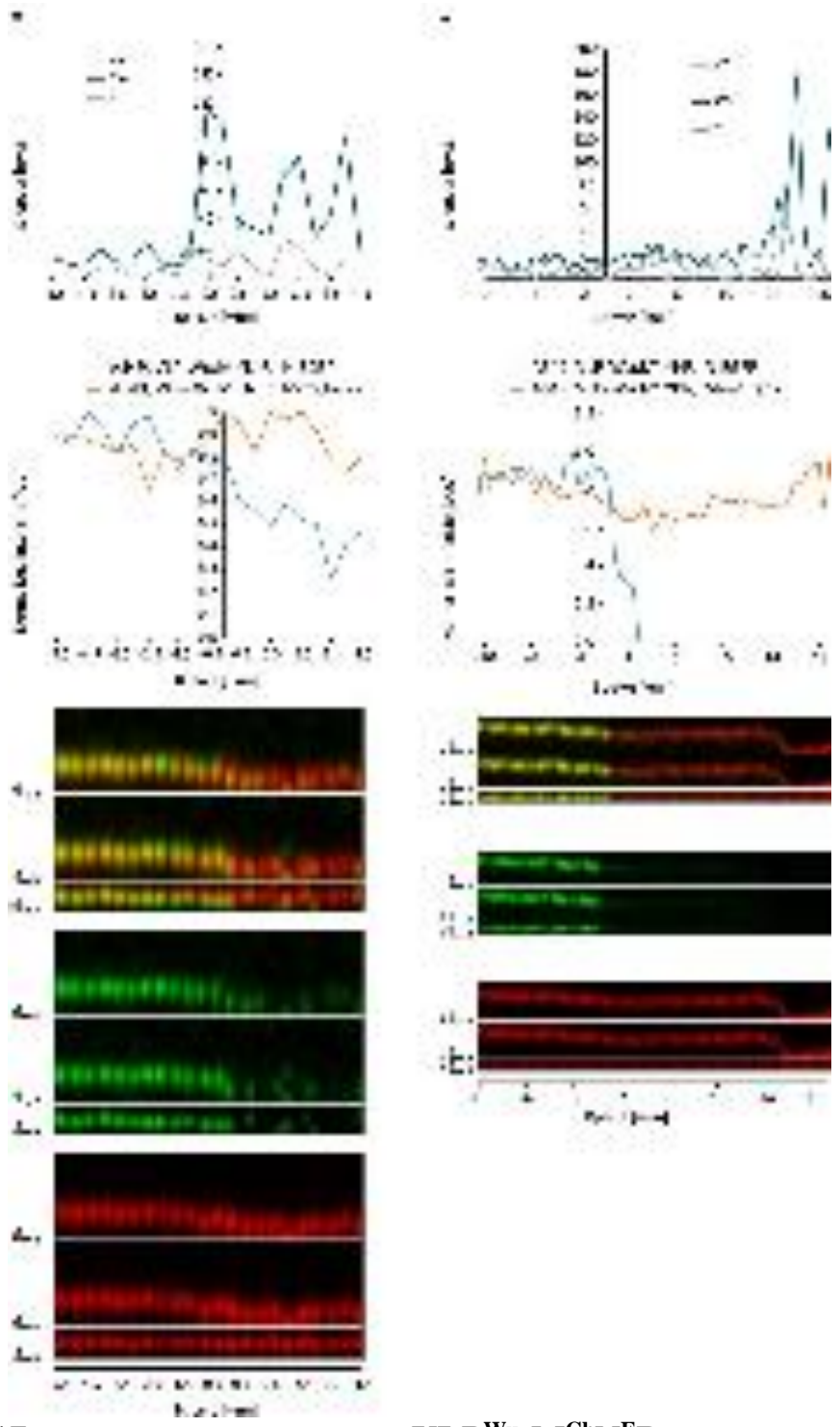
(), N-EGFP M-mCherry.
 M-mCherry N-EGFP
 Z- M-mCherry
 VLP^{Omi}:M^{Ch}N^{eER},
 SARS-CoV-2^{Omicron}:(E, S, M&M-mCherry, N&N-eGFP, T20 RNA).
 VLP^{Wu}:M^{Ch}N^{eER} 2-3% VLP^{Omi}:M^{Ch}N^{eER}. 1%
 VLP^{Omi}:M^{Ch}M^{pHR}- 90%.
 VLP^{Omi}:M^{Ch}N^{eER}, 80%
 N-EGFP mCherry,
 23%
 VLP^{Wu}:M^{Ch}N^{eER} (. 14).
 (. 14).
 N-EGFP
 (. 14).
 (14 , 1).
 (. 14 , , 16 17),
 pH.



16. **VLP^{Omi}:M^{Ch}N^{ER}**

549

A. () (, M-Cherry N-EGFP)
 ()
 N-EGFP
 (),
 EGFP N-



17.

549

VLP^{Wu}:M^{Ch}N^ER

A.

N-EGFP

() () () , M-Cherry N-EGFP
 ()
 () ,
 EGFP () ,
 N-

1). 549 , pH VeroE6 12 , 4 (. 14 ,
 (N-) Rab-5a VeroE6
 549 VeroE6
 SARS-CoV-2 SARS-CoV-2
 del-1 SARS-CoV-2

2.

2.1.

PCNA

HeLa Kyoto chromosome) ⁴¹

MCM6 PCNA, PCNA, mCherry.

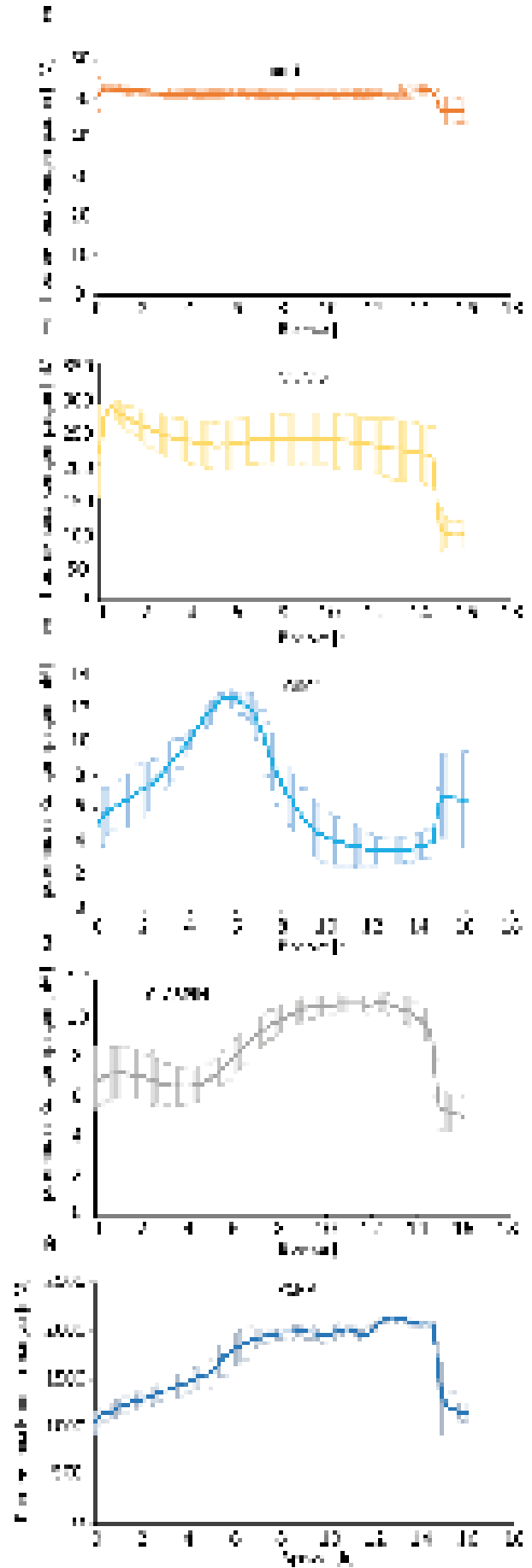
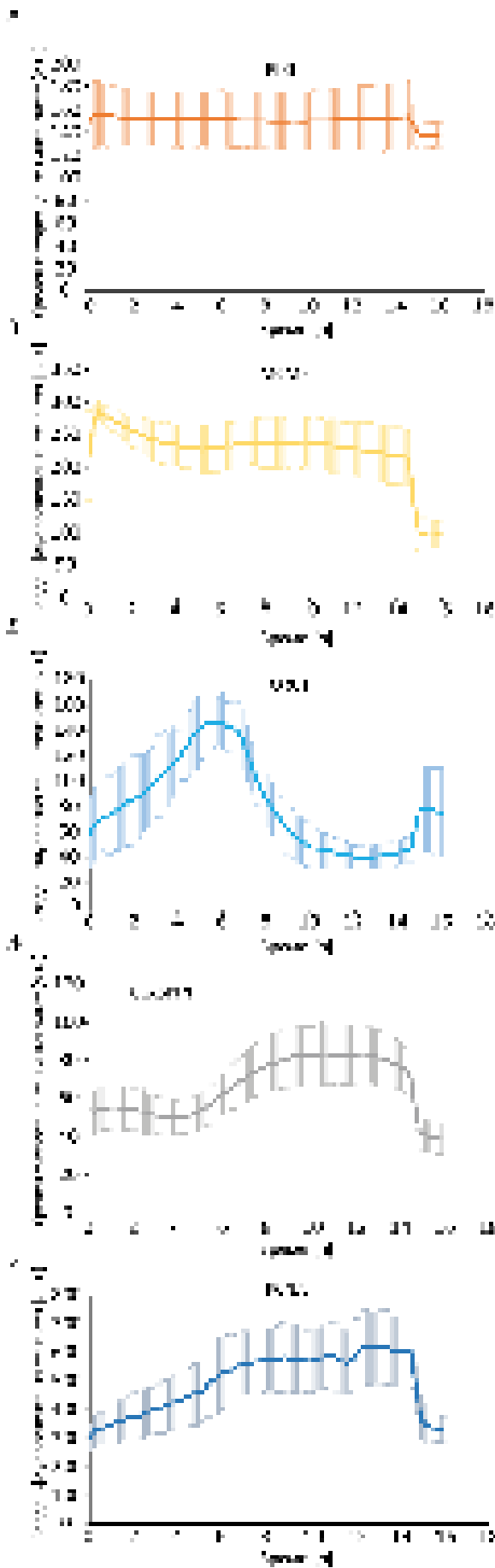
EGFP - ORC1, RIF1, Claspin,

BAC (bacterial artificial

Rif-1, Orc-1, Mcm-6, Claspin

HeLa Kyoto ⁴²

(.18 , , , ,).



18.

PCNA (,) RIF1 (,), MCM6 (,), ORC1 (,), CLASPIN (,)

±

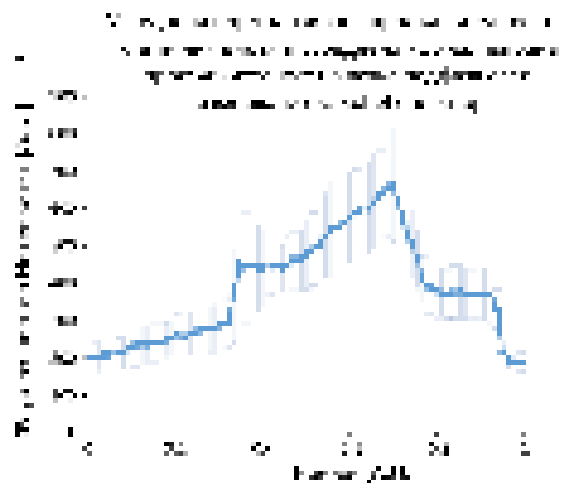
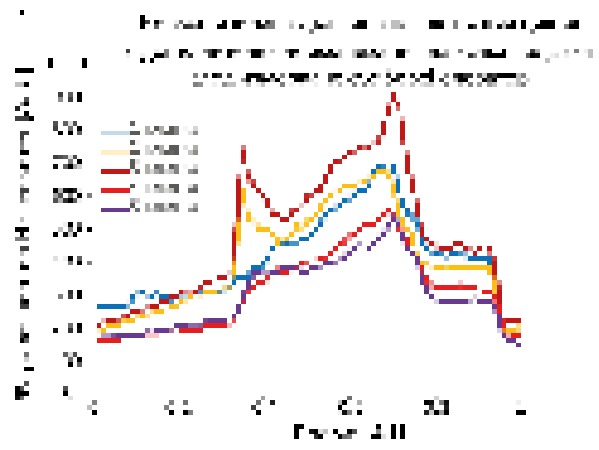
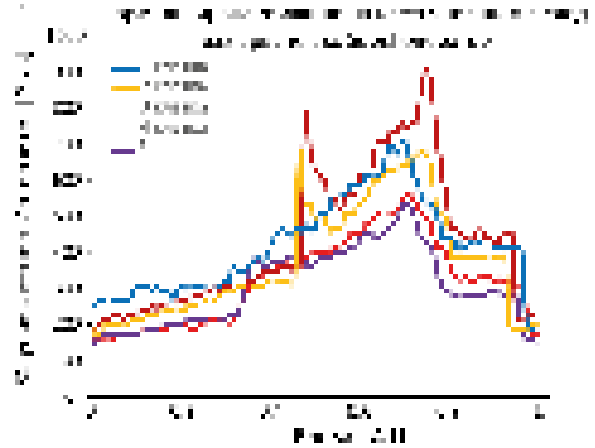
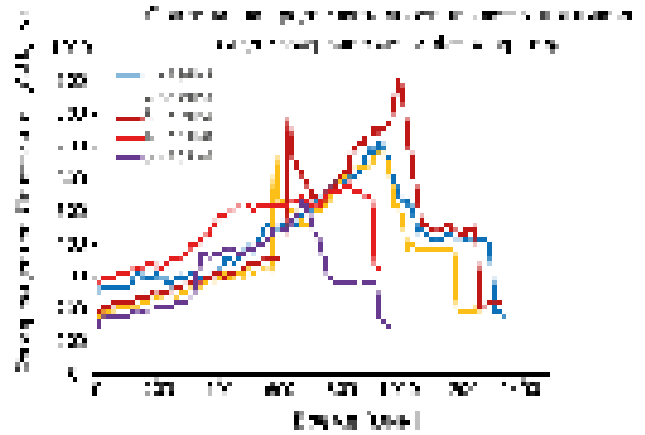
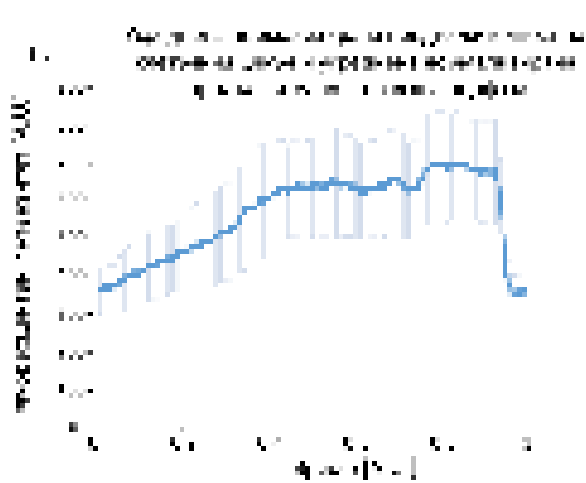
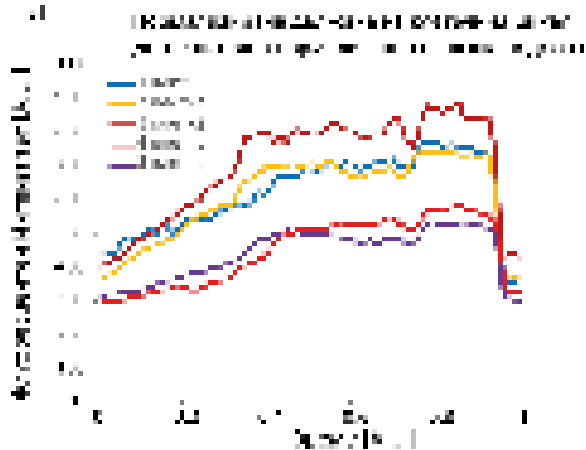
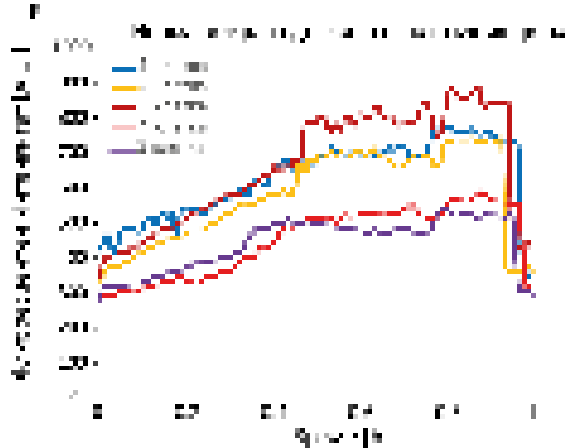
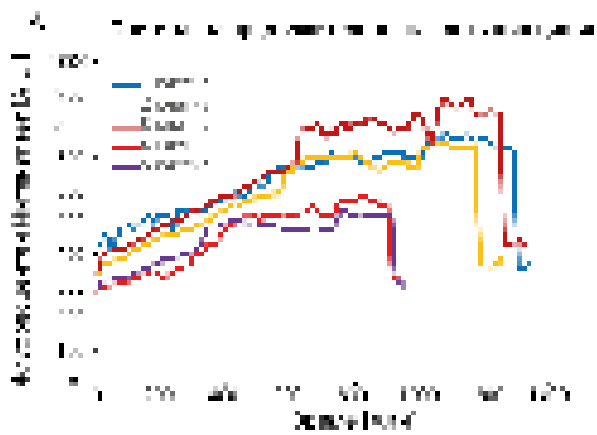
, G1

HeLa Kyoto , 15 h 58 min ± 1 h 56 min.

5 .25 ± 1 13 , S 7 ± 49 , G1 G2 2 38 ± 45
M 55 ± 34 . ,

(. 19).

9.



5 mCherry HeLa Kyoto

() Sobel

() 0 1.

() 0 1.

()

()

()

(n=10)

±

()

(n=10)

±

2.2. PCNA Sobel

, S-

, PCNA

7-9,43

S

S

PCNA-mCherry

mPCNA-mCherry,

hPCNA-EGFP.

20)

(.

PCNA

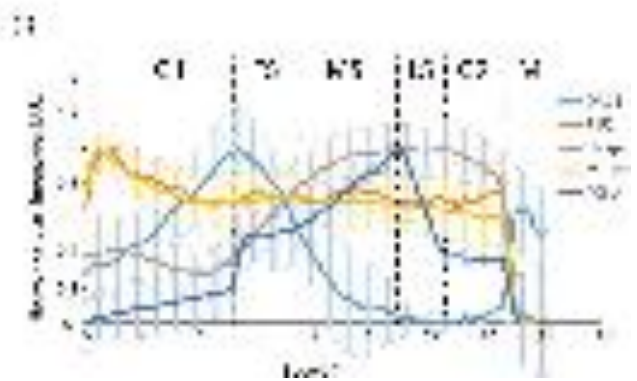
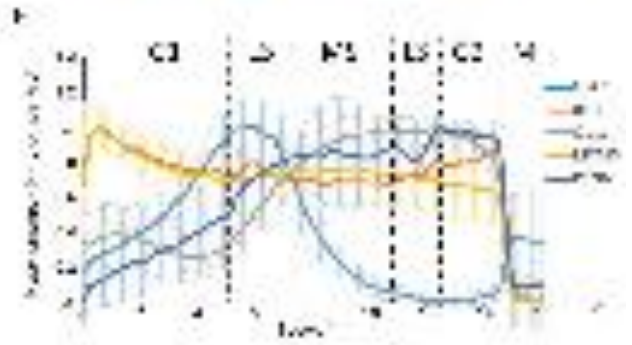
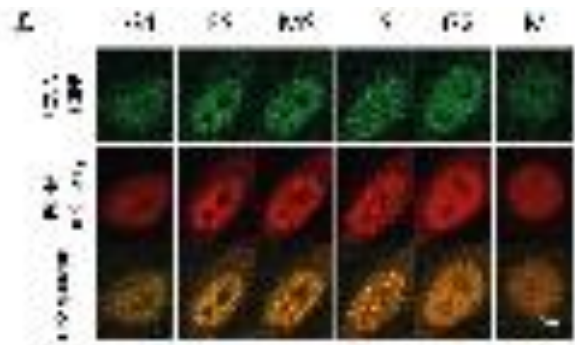
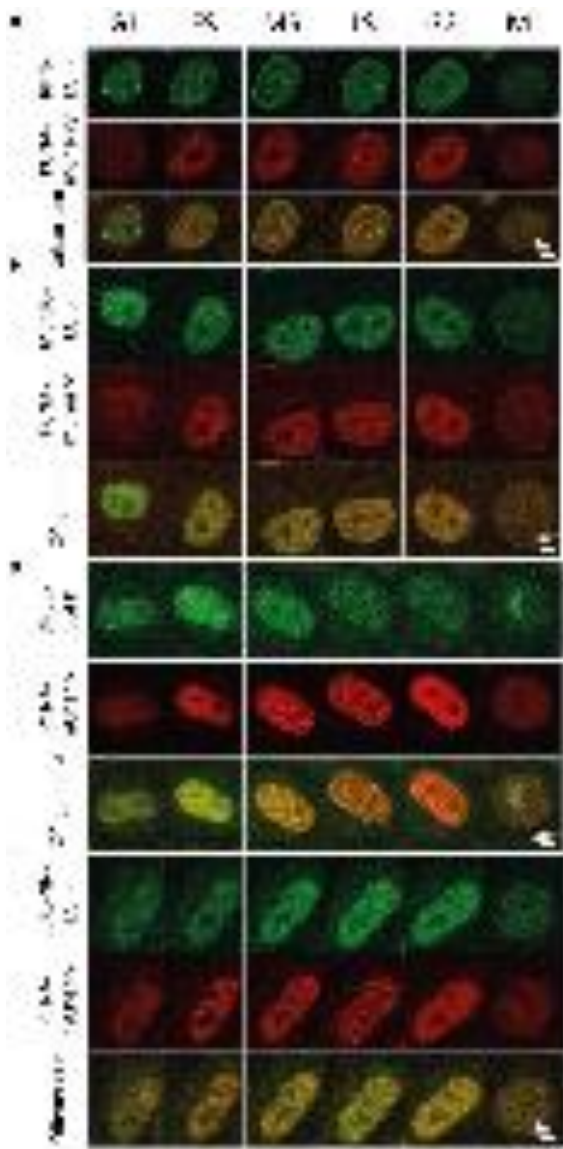
G1

2

G2

(.20 ,

,).



20.

				HeLa Kyoto	,
	RIF1-EGFP	PCNA-mCherry.		HeLa Kyoto	,
	MCM6-EGFP	PCNA-mCherry.		HeLa Kyoto	,
	ORC1-EGFP	PCNA-mCherry.		HeLa Kyoto	,
	CLASPIN-EGFP	PCNA-mCherry.		HeLa Kyoto	,
	PCNA-EGFP	PCNA-mCherry.		HeLa Kyoto	,
S	, LS-	S	15 58	.ES-	S ,MS-
	±				
	()	Sobel			
	±				

PCNA

S

S

Sobel

S

S

Sobel

S

S

(

S

-

),

S -

)

S

-

).

Sobel

(

S

2.3. RIF1

RIF1,

G1

RIF1

PP1

DDK-

44-47

RIF1

RIF1-EGFP/mCherry-PCNA

(.18 ,).

0 1,

, RIF1 G1

. 30 - , G1 ,

(. 20 , , . 21). , G1 S , RIF1

,
44-47. Sobel

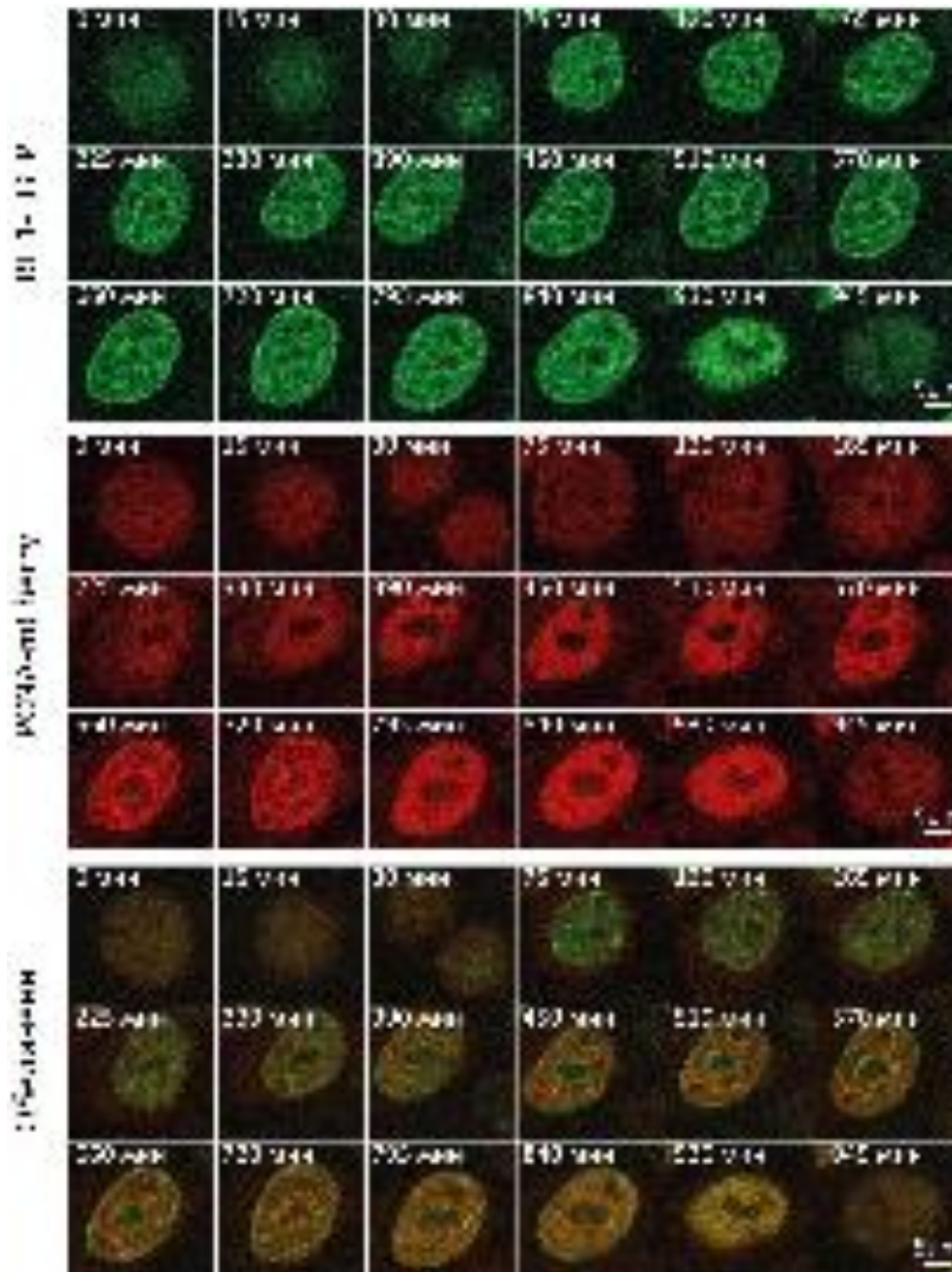
(. 20). ,

, G1 G2 , RIF1

, G1 , RIF1 . S

, G1 M

.



21.

RIF1-EGFP/mCherry-PCNA HeLa Kyoto

2.4. MCM6

MCM6

RIF1 MCM6

44,

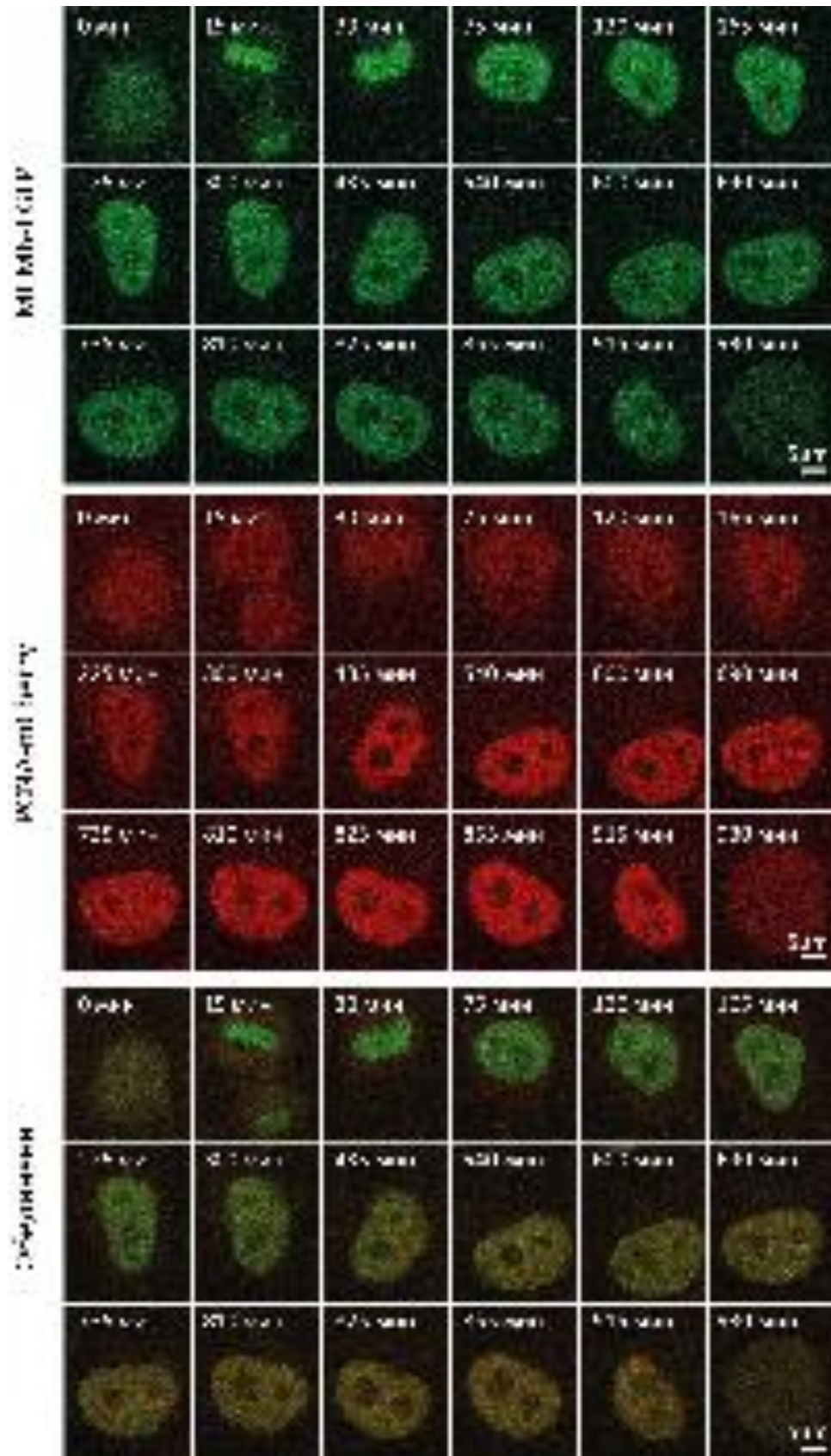
MCM6

RIF1. MCM6

MCM2-7

CM2-7

- ORC ,
 48,49 . RIF1
 MCM6
 (. 18 ,). MCM6
 RIF1 .
 MCM6 G1 30- ,
 S G2 (. 20 ,). ,
 , G1 , 100 S ,
 300 . ,
 (. 22). ,
 G1 -
 , G1 MCM6, .
 , - S ,
 . RIF1,
 S G2 , MCM6 .
 S . , MCM6,
 , - .



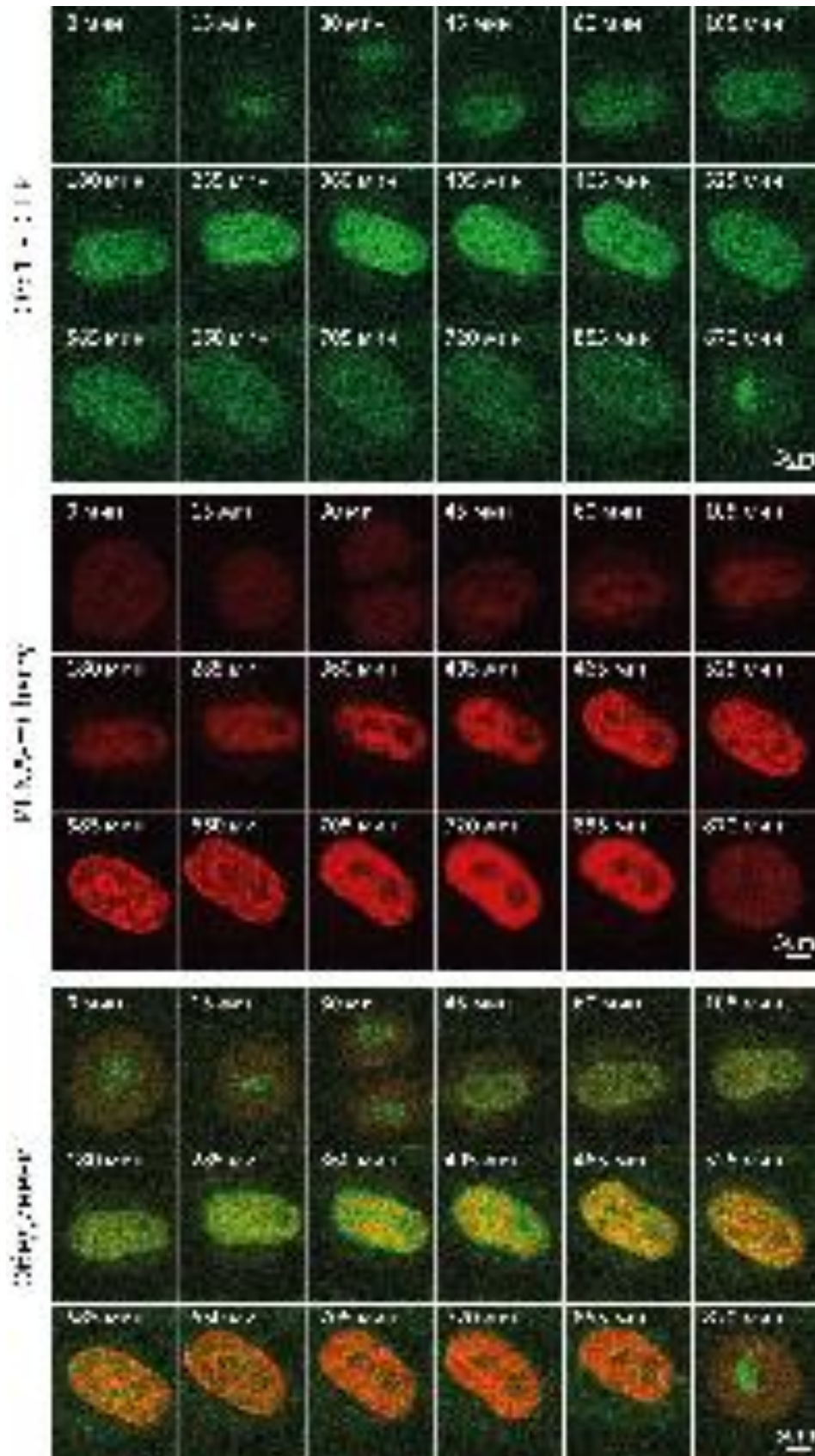
22.

MCM6-EGFP/mCherry-PCNA HeLa

Kyoto

2.5. ORC1

,
 - ORC1. - origin recognition complex
 (ORC).
 ,
 CDC6 CDT1 S MCM2-7 . ORC,
 - 50,51.
 S , ORC1
 G2 ⁵².
 , ORC1
 (.20 ,).
 G1 ,
 2 , S
 G2 (. 20 . 23).
 , PCNA-mCherry,
 - S ,
 ,
 G2 ,
 G2 , 50-55.
 ORC1



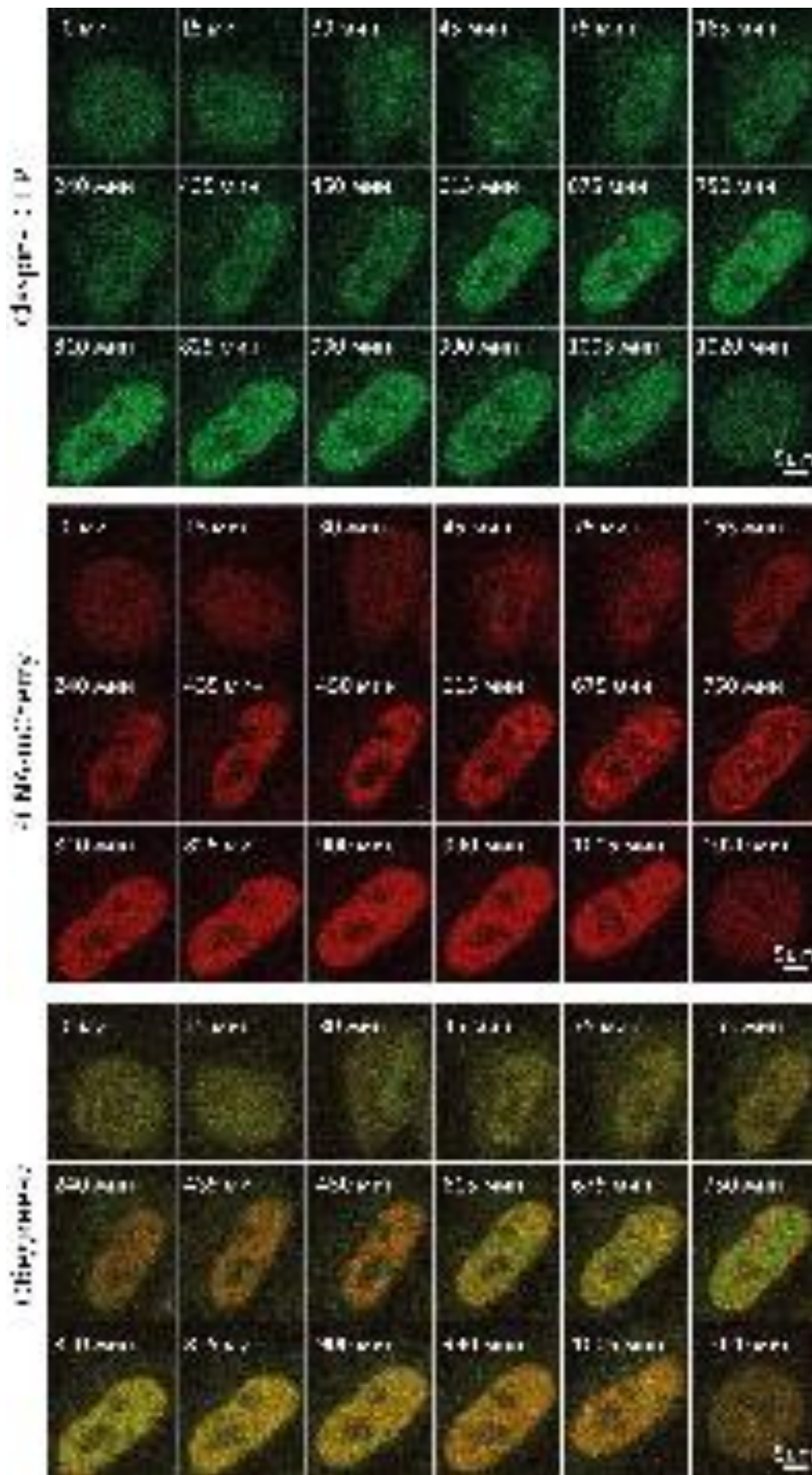
23.

ORC1-EGFP/mCherry-PCNA HeLa

Kyoto

2.6. CLASPIN

Claspin, ATR-⁵⁶, CL SPIN, Chk1, (Origin Firing)⁵⁷, G1, G2⁵⁸, CLASPIN, G1, S, S, (.20 , 24), .20, ORC1, ORC1, M, -



24.

CLASPIN-EGFP/mCherry-PCNA

HeLa Kyoto

.

RIF1
M/G1 G2/M
M. , MCM6
2 3 RIF1.
G1, MCM6 MCM6
S . S ,
, , - -
, ORC1 , MCM6,
G1 , S
M . , ,
, , CLASPIN S ,
S , G2/M.
, ,
, .

3.

(40 B)

<https://covidynamics.imb.bas.bg/>.

„DNArepairK: An interactive database for exploring the impact of anticancer drugs onto the dynamics of DNA repair proteins“.

V.

1.

SPARTACUSS
(X,Y Z),
SPARTACUSS
15 30
SPARTACUSS
: 1)
; 2)
; 3) e
(

<https://covidynamics.imb.bas.bg/> „DNArepairK: An interactive database for exploring the impact of anticancer drugs onto the dynamics of DNA repair proteins.

2.

<https://covidynamics.imb.bas.bg/> „DNArepairK: An interactive database for exploring the impact of anticancer drugs onto the dynamics of DNA repair proteins

3.

SARS-CoV-

2

SARS-CoV-2

pH

: 1)

, 3)

-1

, 2)

, 4)

5)

, 4

VeroE6

12

A549

pH-

pH-

-1

(

N-

)

Rab5a

A549 SARS-CoV-2 pH Ver0E6 Ver0E6
 SARS-CoV-2 59-63
 Ver0E6 32,64-66
 SARS-CoV-2 ACE2
 TMPRSS2, pH
 (pH)
 TMPRSS2 ACE2, 67,68
 del-1 S SARS-CoV-
 Ver0E6
 S1/S2 S 37,69
 Furin Furin

Omicron

-

4.

S

70-72

PCNA

Sobel

G1,

S,

S,

S, G2

M

RIF1

G1

44,

G1

44,73-75

RIF1

(. 20,21) MCM6

G1,

RIF1

-

G1

76-78

MCM

MCM6⁷⁹⁻⁸¹, MCM6
 G1, S,
 PCNA., PCNA.
 ORC1,
 ORC^{50,51,53},
 S
 G1,
 S
 Orc1, S,
 Claspin,
 S^{57,82-84}. Claspin,
 S,
 S,
 Orc1, M,
 Orc1,
 Orc1,
 Orc1

' SARS-CoV-2 '

-

,

.

,

,

.

,

,

,

,

,

,

.

VI.

1. SARS-CoV-2 -
2. -
3. pH SARS-CoV-2 -
4. SARS-CoV-2 S -
5. SARS-CoV-2 - RAb5a
6. Omicron SARS-CoV-2 (del-1) / S SARS-COV-2 -
7. pH, A549, VeroE6 -
8. CLASPIN, PCNA RIF1, ORC1, MCM6,

1. SARS-CoV-2
2. -
3. G1, G2 M , S, S S

PCNA

4. Sobel COVIDynamics DNAREPAIRK Database,

SARS-CoV-2

5.

5

pH,

1. Aleksandar Ategin, Anelia Ivanova, Wiley Peppel, Rumen Stamatov, Rodrigo Gallegos, Haley Durden, Sonya Uzunova, Michael D. Vershinin, Saveez Saffarian and Stoyno S. Stoyanov. **“Kinetic landscape of single virus-like particles highlights the efficacy of SARS-Cov-2 internalization”**. *Viruses*. Impact Factor: **3.8 (2023)**
2. Aleksandar Sergeev Ategin, Aneliya Ivanova, Petar-Bogomil Kanev, Sonya Uzunova, Marina Nedelcheva-Veleva, Stoyno Stoyanov. **“Dynamics of replication-associated protein levels through the cell cycle”**. *IJMS*. Impact Factor: **4.9 (2023)**
3. Babukov, Y., Aleksandrov, R., Ivanova, A., Ategin, A., & Stoyanov, S. **“DNArepairK: An interactive database for exploring the impact of anticancer drugs onto the dynamics of DNA repair proteins”** *Biomedicines*, 9(9), 1238. Impact Factor: **4.757 (2021)**

1. Radoslav Aleksandrov, Anton Dotchev, Ina Poser, Dragomir Krastev, Georgi Georgiev, Greta Panova, Yordan Babukov, Georgi Danovski, Teodora Dyankova, Lars Hubatsch, Aneliya Ivanova, Aleksandar Ategin, Marina N. Nedelcheva-Veleva, Susanne Hasse, Mihail Sarov, Frank Buchholz, Anthony A. Hyman, Stephan W. Grill, Stoyno S. Stoyanov. **“Protein Dynamics in Complex DNA Lesions”**. (2018). *Molecular cell*. 69(6). 1046-1061. Impact Factor: **14.548 (2018)**.
2. Kanev, P. B., Ategin, A., Stoyanov, S., & Aleksandrov, R. (2023, September). **“PARP1 roles in DNA repair and DNA replication: The basi(c)s of PARP inhibitor efficacy and resistance”**. In *Seminars in Oncology*. WB Saunders. Impact Factor: **3.0 (2023)**.
3. Ivanova, A., Ategin, A., Uzunova, S., Danovski, G., Aleksandrov, R., Stoyanov, S., & Nedelcheva-Veleva, M. (2021). **“The effect of Dia2 protein deficiency on the cell cycle, cell size, and recruitment of Ctf4 protein in *Saccharomyces cerevisiae*”**. *Molecules*, 27(1), 97. Impact Factor: **4.927 (2021)**.

1. 2024 A.Ategin et al.”Dynamics of replication-associated protein levels through the cell cycle”, EMBO Conference,

2. 2023 A.Atemin et al. „Kinetics of SARS-CoV-2 entry into cells“, IPols,
3. 2022 A.Atemin et al. “Kinetics of SARS-CoV-2 entry into cells”, „100“
4. 2020 A.Atemin et al. “Dia2 at the crossroad between DNA replication and cell’s size homeostasis.”, IPols, (
5. 2019 A.Atemin et al. “The fine-tuned balance between expression and degradation regulates the cell fate”, ECHG,
6. 2019 A.Atemin et al. “Analysis of the key replication protein Claspin and its yeast analogue Ctf4”,
7. 2019 A.Atemin et al. “Dynamic Changes in the Replication Complex During Normal and Perturbed Replication”, Humbolt Kolleg,
8. 2018 A.Atemin et al. “Ctf4 in the context of replication”, FEBS 2018,
9. 2017 A.Atemin et al. “Dynamic Changes in the Replication Complex During Normal and Perturbed Replication”, ICGEB,
- 10.2017 A.Atemin et al. “Dia2-mediated control of Ctf4 in the context of replication complex integrity”, FEBS 2017,
- 11.2016 A.Atemin et al. “Ctf4 dynamics”,

1. Poser, I. *et al.* BAC TransgeneOmics: a high-throughput method for exploration of protein function in mammals. *Nat. Methods* **5**, 409–415 (2008).
2. Song, B. D., Yarar, D. & Schmid, S. L. An assembly-incompetent mutant establishes a requirement for dynamin self-assembly in clathrin-mediated endocytosis in vivo. *Mol. Biol. Cell* **15**, 2243–2252 (2004).
3. Swann, H. *et al.* Minimal system for assembly of SARS-CoV-2 virus like particles. *Sci. Rep.* **10**, 1–5 (2020).
4. Gourdelier, M. *et al.* Optimized production and fluorescent labeling of SARS-CoV-2 virus-like particles. *Sci. Rep.* **12**, 1–15 (2022).
5. Sankaranarayanan, S., De Angelis, D., Rothman, J. E. & Ryan, T. A. The use of pHluorins for optical measurements of presynaptic activity. *Biophys. J.* **79**, 2199–2208 (2000).
6. Kurki, P., Vanderlaan, M., Dolbeare, F., Gray, J. & Tan, E. M. Expression of proliferating cell nuclear antigen (PCNA)/cyclin during the cell cycle. *Exp. Cell Res.* **166**, 209–219 (1986).
7. Somanathan, S., Suchyna, T. M., Siegel, A. J. & Berezney, R. Targeting of PCNA to sites of DNA replication in the mammalian cell nucleus*. *J. Cell. Biochem.* **81**, 56–67 (2001).
8. Schonenberger, F., Deutzmann, A., Ferrando-May, E. & Merhof, D. Discrimination of cell cycle

- phases in PCNA-immunolabeled cells. *BMC Bioinformatics* **16**, 180 (2015).
9. Sasaki, K., Kurose, A. & Ishida, Y. Flow cytometric analysis of the expression of PCNA during the cell cycle in hela cells and effects of the inhibition of DNA synthesis on it. *Cytometry* **14**, 876–882 (1993).
 10. Danovski, G. *et al.* CellTool: An Open-Source Software Combining Bio-Image Analysis and Mathematical Modeling for the Study of DNA Repair Dynamics. *Int. J. Mol. Sci.* **24**, (2023).
 11. Schindelin, J. *et al.* Fiji - an Open platform for biological image analysis. *Nat. Methods* **9**, (2009).
 12. Tan, E., Chin, C. S. H., Lim, Z. F. S. & Ng, S. K. HEK293 Cell Line as a Platform to Produce Recombinant Proteins and Viral Vectors. *Front. Bioeng. Biotechnol.* **9**, 1–9 (2021).
 13. Sharma, A. *et al.* Structural stability of SARS-CoV-2 virus like particles degrades with temperature. *Biochem. Biophys. Res. Commun.* **534**, 343–346 (2021).
 14. Xu, R., Shi, M., Li, J., Song, P. & Li, N. Construction of SARS-CoV-2 Virus-Like Particles by Mammalian Expression System. *Front. Bioeng. Biotechnol.* **8**, 1–6 (2020).
 15. Zhang, Y. *et al.* Single particle tracking reveals SARS-CoV-2 regulating and utilizing dynamic filopodia for viral invasion. *Sci. Bull.* **68**, 2210–2224 (2023).
 16. Huang, R. *et al.* Betanodavirus-like particles enter host cells via clathrin-mediated endocytosis in a cholesterol-, pH- and cytoskeleton-dependent manner. *Vet. Res.* **48**, 1–17 (2017).
 17. Zepeda-Cervantes, J., Ramírez-Jarquín, J. O. & Vaca, L. Interaction Between Virus-Like Particles (VLPs) and Pattern Recognition Receptors (PRRs) From Dendritic Cells (DCs): Toward Better Engineering of VLPs. *Front. Immunol.* **11**, 1–22 (2020).
 18. Ogando, N. S. *et al.* SARS-coronavirus-2 replication in Vero E6 cells: Replication kinetics, rapid adaptation and cytopathology. *J. Gen. Virol.* **101**, 925–940 (2020).
 19. Prichard, K. L., O'Brien, N. S., Murcia, S. R., Baker, J. R. & McCluskey, A. Role of Clathrin and Dynamin in Clathrin Mediated Endocytosis/Synaptic Vesicle Recycling and Implications in Neurological Diseases. *Front. Cell. Neurosci.* **15**, (2022).
 20. Cocucci, E., Gaudin, R. & Kirchhausen, T. Dynamin recruitment and membrane scission at the neck of a clathrin-coated pit. *Mol. Biol. Cell* **25**, 3595–3609 (2014).
 21. Antonny, B. *et al.* Membrane fission by dynamin: what we know and what we need to know. *EMBO J.* **35**, 2270–2284 (2016).
 22. Cheng, X. *et al.* Dynamin-dependent vesicle twist at the final stage of clathrin-mediated endocytosis. *Nat. Cell Biol.* **23**, 859–869 (2021).
 23. Hill, E., Van Der Kaay, J., Downes, C. P. & Smythe, E. The role of dynamin and its binding partners in coated pit invagination and scission. *J. Cell Biol.* **152**, 309–323 (2001).
 24. Štimac, I. *et al.* Dynamin inhibitors prevent the establishment of the cytomegalovirus assembly compartment in the early phase of infection. *Life* **11**, (2021).
 25. Loerke, D. *et al.* Cargo and dynamin regulate clathrin-coated pit maturation. *PLoS Biol.* **7**, 0628–0639 (2009).
 26. Wang, C. *et al.* Investigation of endosome and lysosome biology by ultra pH-sensitive nanoprobe. *Adv. Drug Deliv. Rev.* **113**, 87–96 (2017).

27. Yang, Y., Mengran Yu, Zhang, S., Ma, G. & Su, Z. Adsorption of virus-like particles on ion exchange surface: Conformational changes at different pH detected by dual polarization interferometry. *J. Chromatogr. A* **1408**, 161–168 (2015).
28. Ausar, S. F., Foubert, T. R., Hudson, M. H., Vedvick, T. S. & Middaugh, C. R. conformational stability and disassembly of norwalk virus-like particles: Effect of ph and temperature. *J. Biol. Chem.* **281**, 19478–19488 (2006).
29. Maassen, S. J., van der Schoot, P. & Cornelissen, J. J. L. M. Experimental and Theoretical Determination of the pH inside the Confinement of a Virus-Like Particle. *Small* **14**, 1–7 (2018).
30. Martineau, M. *et al.* Semisynthetic fluorescent pH sensors for imaging exocytosis and endocytosis. *Nat. Commun.* **8**, 1–10 (2017).
31. Syed, A. M. *et al.* Rapid assessment of SARS-CoV-2–evolved variants using virus-like particles. *Science (80-.).* **374**, 1626–1632 (2021).
32. Rossi, G. A., Sacco, O., Mancino, E., Cristiani, L. & Midulla, F. Differences and similarities between SARS-CoV and SARS-CoV-2: spike receptor-binding domain recognition and host cell infection with support of cellular serine proteases. *Infection* **48**, 665–669 (2020).
33. Lau, S. Y. *et al.* Attenuated SARS-CoV-2 variants with deletions at the S1/S2 junction. *Emerg. Microbes Infect.* **9**, 837–842 (2020).
34. Sasaki, M. *et al.* SARS-CoV-2 variants with mutations at the S1/ S2 cleavage site are generated in vitro during propagation in TMPRSS2-deficient cells. *PLoS Pathog.* **17**, 1–17 (2021).
35. Harvey, W. T. *et al.* SARS-CoV-2 variants, spike mutations and immune escape. *Nat. Rev. Microbiol.* **19**, 409–424 (2021).
36. Peacock, T. P. *et al.* The furin cleavage site in the SARS-CoV-2 spike protein is required for transmission in ferrets. *Nat. Microbiol.* **6**, 899–909 (2021).
37. Lubinski, B. & Whittaker, G. R. The SARS-CoV-2 furin cleavage site: natural selection or smoking gun? *The Lancet Microbe* **4**, e570 (2023).
38. Hoffmann, M., Kleine-Weber, H. & Pöhlmann, S. A Multibasic Cleavage Site in the Spike Protein of SARS-CoV-2 Is Essential for Infection of Human Lung Cells. *Mol. Cell* **78**, 779-784.e5 (2020).
39. Hui, K. P. Y. *et al.* SARS-CoV-2 Omicron variant replication in human bronchus and lung ex vivo. *Nature* **603**, 715–720 (2022).
40. Syed, A. M. *et al.* Omicron mutations enhance infectivity and reduce antibody neutralization of SARS-CoV-2 virus-like particles. *Proc. Natl. Acad. Sci. U. S. A.* **119**, 1–7 (2022).
41. Poser, I. *et al.* BAC TransgeneOmics: a high-throughput method for exploration of protein function in mammals. *Nat Methods* **5**, 409–415 (2008).
42. Raghuraman, B. K. *et al.* Median-Based Absolute Quantification of Proteins Using Fully Unlabeled Generic Internal Standard (FUGIS). *J. Proteome Res.* **21**, 132–141 (2022).
43. Essers, J. *et al.* Nuclear dynamics of PCNA in DNA replication and repair. *Mol Cell Biol* **25**, 9350–9359 (2005).
44. Hiraga, S. I. *et al.* Rif1 controls DNA replication by directing Protein Phosphatase 1 to reverse Cdc7-mediated phosphorylation of the MCM complex. *Genes Dev.* **28**, 372–383 (2014).

45. Hiraga, S. *et al.* Human RIF1 and protein phosphatase 1 stimulate DNA replication origin licensing but suppress origin activation. *EMBO Rep.* e201641983 (2017) doi:10.15252/embr.201641983.
46. Foti, R. *et al.* Nuclear Architecture Organized by Rif1 Underpins the Replication-Timing Program. *Mol. Cell* **61**, 260–273 (2016).
47. Malzl, D. *et al.* RIF1 regulates early replication timing in murine B cells. *Nat. Commun.* **14**, 1–18 (2023).
48. Symeonidou, I. E. *et al.* Multi-step loading of human minichromosome maintenance proteins in live human cells. *J. Biol. Chem.* **288**, 35852–35867 (2013).
49. Deegan, T. D., Mukherjee, P. P., Fujisawa, R., Polo Rivera, C. & Labib, K. CMG helicase disassembly is controlled by replication fork DNA, replisome components and a ubiquitin threshold. *Elife* **9**, (2020).
50. Tatsumi, Y., Ohta, S., Kimura, H., Tsurimoto, T. & Obuse, C. The ORC1 cycle in human cells: I. Cell cycle-regulated oscillation of human ORC1. *J. Biol. Chem.* **278**, 41528–41534 (2003).
51. Ohta, S., Tatsumi, Y., Fujita, M., Tsurimoto, T. & Obuse, C. The ORC1 cycle in human cells: II. Dynamic changes in the human ORC complex during the cell cycle. *J. Biol. Chem.* **278**, 41535–41540 (2003).
52. Kara, N., Hossain, M., Prasanth, S. G. & Stillman, B. Orc1 binding to mitotic chromosomes precedes spatial patterning during G1 phase and assembly of the origin recognition complex in human cells. *J. Biol. Chem.* **290**, 12355–12369 (2015).
53. DePamphilis, M. L. The ‘ORC cycle’: A novel pathway for regulating eukaryotic DNA replication. *Gene* **310**, 1–15 (2003).
54. Méndez, J. & Stillman, B. Chromatin Association of Human Origin Recognition Complex, Cdc6, and Minichromosome Maintenance Proteins during the Cell Cycle: Assembly of Prereplication Complexes in Late Mitosis. *Mol. Cell. Biol.* **20**, 8602–8612 (2000).
55. Kreitz, S., Ritzi, M., Baack, M. & Knippers, R. The Human Origin Recognition Complex Protein 1 Dissociates from Chromatin during S Phase in HeLa Cells. *J. Biol. Chem.* **276**, 6337–6342 (2001).
56. Peschiaroli, A. *et al.* SCFbetaTrCP-mediated degradation of Claspin regulates recovery from the DNA replication checkpoint response. *Mol Cell* **23**, 319–329 (2006).
57. Hsiao, H.-W., Yang, C.-C. & Masai, H. Roles of Claspin in regulation of DNA replication, replication stress responses and oncogenesis in human cells. *Genome Instab. Dis.* **2**, 263–280 (2021).
58. Bennett, L. N. & Clarke, P. R. Regulation of Claspin degradation by the ubiquitin-proteasome pathway during the cell cycle and in response to ATR-dependent checkpoint activation. *FEBS Lett.* **580**, 4176–4181 (2006).
59. Hou, Y. J. *et al.* SARS-CoV-2 Reverse Genetics Reveals a Variable Infection Gradient in the Respiratory Tract. *Cell* **182**, 429-446.e14 (2020).
60. Essaidi-Laziosi, M. *et al.* Estimating clinical SARS-CoV-2 infectiousness in Vero E6 and primary airway epithelial cells. *The Lancet Microbe* **2**, e571 (2021).
61. Melis, R., Braca, A., Pagnozzi, D. & Anedda, R. The metabolic footprint of Vero E6 cells highlights the key metabolic routes associated with SARS-CoV-2 infection and response to drug combinations. *Sci. Rep.* **14**, 1–12 (2024).

62. Aiweesakun, P. *et al.* Systematic Exploration of SARS-CoV-2 Adaptation to Vero E6, Vero E6/TMPRSS2, and Calu-3 Cells. *Genome Biol. Evol.* **15**, 1–21 (2023).
63. Ogando, N. S. *et al.* SARS-coronavirus-2 replication in Vero E6 cells: replication kinetics, rapid adaptation and cytopathology. *J. Gen. Virol.* **101**, 925–940 (2020).
64. Emeny, J. M. & Morgan, M. J. Regulation of the interferon system: evidence that Vero cells have a genetic defect in interferon production. *J. Gen. Virol.* **43**, 247–252 (1979).
65. Wang, L. *et al.* Susceptibility to SARS-CoV-2 of cell lines and substrates commonly used to diagnose and isolate influenza and other viruses. *Emerg. Infect. Dis.* **27**, 1380–1392 (2021).
66. Cagno, V. SARS-CoV-2 cellular tropism. *The Lancet Microbe* **1**, e2–e3 (2020).
67. Letoha, A., Hudák, A. & Letoha, T. Exploring the Syndecan-Mediated Cellular Internalization of the SARS-CoV-2 Omicron Variant. *Int. J. Mol. Sci.* **24**, (2023).
68. Hudák, A., Letoha, A., Szilák, L. & Letoha, T. Contribution of syndecans to the cellular entry of SARS-CoV-2. *Int. J. Mol. Sci.* **22**, 1–27 (2021).
69. Hoffmann, M., Kleine-Weber, H. & Pöhlmann, S. A Multibasic Cleavage Site in the Spike Protein of SARS-CoV-2 Is Essential for Infection of Human Lung Cells. *Mol. Cell* **78**, 779-784.e5 (2020).
70. Nicolini, C., Kendall, F. & Giaretti, W. Objective identification of cell cycle phases and subphases by automated image analysis. *Biophys. J.* **19**, 163–176 (1977).
71. Zerjatke, T. *et al.* Quantitative Cell Cycle Analysis Based on an Endogenous All-in-One Reporter for Cell Tracking and Classification. *Cell Rep.* **19**, 1953–1966 (2017).
72. Guo, X. & Chen, L. From G1 to M: a comparative study of methods for identifying cell cycle phases. *Brief. Bioinform.* **25**, 1–10 (2024).
73. Noordermeer, S. M. *et al.* The shieldin complex mediates 53BP1-dependent DNA repair. *Nature* **560**, 117–121 (2018).
74. Ochs, F. *et al.* Stabilization of chromatin topology safeguards genome integrity. *Nature* **574**, 571–574 (2019).
75. Gnan, S. *et al.* Nuclear organisation and replication timing are coupled through RIF1–PP1 interaction. *Nat. Commun.* **12**, 1–10 (2021).
76. Masai, H., Matsumoto, S., You, Z., Yoshizawa-Sugata, N. & Oda, M. Eukaryotic chromosome DNA replication: where, when, and how? *Annu Rev Biochem* **79**, 89–130 (2010).
77. Cheng, L. *et al.* Expression Profile and Prognostic Values of Mini-Chromosome Maintenance Families (MCMs) in Breast Cancer. *Med. Sci. Monit. Int. Med. J. Exp. Clin. Res.* **26**, e923673 (2020).
78. Symeonidou, I. E. *et al.* Multi-step loading of human minichromosome maintenance proteins in live human cells. *J Biol Chem* **288**, 35852–35867 (2013).
79. Liu, Z. *et al.* MCM family in HCC: MCM6 indicates adverse tumor features and poor outcomes and promotes S/G2 cell cycle progression. *BMC Cancer* **18**, 200 (2018).
80. Blow, J. J. & Dutta, A. Preventing re-replication of chromosomal DNA. *Nat Rev Mol Cell Biol* **6**, 476–486 (2005).

81. Komata, M., Bando, M., Araki, H. & Shirahige, K. The Direct Binding of Mrc1, a Checkpoint Mediator, to Mcm6, a Replication Helicase, Is Essential for the Replication Checkpoint against Methyl Methanesulfonate-Induced Stress. *Mol. Cell. Biol.* **29**, 5008–5019 (2009).
82. Bareti, D. *et al.* Cryo-EM Structure of the Fork Protection Complex Bound to CMG at a Replication Fork. *Mol. Cell* **78**, 926-940.e13 (2020).
83. Lou, H. *et al.* Mrc1 and DNA Polymerase δ Function Together in Linking DNA Replication and the S Phase Checkpoint. *Mol. Cell* **32**, 106–117 (2008).
84. Kumagai, A. & Dunphy, W. G. Claspin, a novel protein required for the activation of Chk1 during a DNA replication checkpoint response in *Xenopus* egg extracts. *Mol. Cell* **6**, 839–849 (2000).